Fluvial incision into bedrock: Insights from morphometric analysis and numerical modeling of gorges incising glacial hanging valleys (Western Alps, France)

Pierre Valla, Peter A. Van Der Beek, Dimitri Lague

JOURNAL OF GEOPHYSICAL RESEARCH, VOL. 115, F02010, doi:10.1029/2008JF001079, 2010

Fluvial incision into bedrock: Insights from morphometric analysis and numerical modeling of gorges incising glacial hanging valleys (Western Alps, France)

Pierre G. Valla,[1] Peter A. van der Beek,[1] and Dimitri Lague[2]

Received 21 May 2008; revised 12 November 2009; accepted 23 November 2009; published 4 May 2010.

[1] Bedrock gorges incising glacial hanging valleys potentially allow measurements of fluvial bedrock incision in mountainous relief. Using digital elevation models, topographic maps, and field reconnaissance, we identified and characterized 30 tributary hanging valleys incised by gorges near their confluence with trunk streams in the Romanche watershed, French Western Alps. Longitudinal profiles of these tributaries are all convex and have abrupt knickpoints at the upper limit of oversteepened gorge reaches. We reconstructed initial glacial profiles from glacially polished bedrock knobs surrounding the gorges in order to quantify the amount of fluvial incision and knickpoint retreat. From morphometric analyses, we find that mean channel gradients and widths, as well as knickpoint retreat rates, display a drainage area dependence modulated by bedrock lithology. However, there appears to be no relation between horizontal retreat and vertical downwearing of knickpoints. Assuming a postglacial origin of these gorges, our results imply high postglacial fluvial incision (0.5–15 mm yr^{-1}) and knickpoint retreat (1–200 mm yr^{-1}) rates that are, however, consistent with previous estimates. Numerical modeling was used to test the capacity of different fluvial incision models to predict the inferred evolution of the gorges. Results from simple end-member models suggest transport-limited behavior of the bedrock gorges. A more sophisticated model including dynamic width adjustment and sediment-dependent incision rates predicts present-day channel geometry only if a significant supply of sediment from the gorge sidewalls (~10 mm yr^{-1}) is triggered by gorge deepening, combined with pronounced inhibition of bedrock incision by sediment transport and deposition.

Citation: Valla, P. G., P. A. van der Beek, and D. Lague (2010), Fluvial incision into bedrock: Insights from morphometric analysis and numerical modeling of gorges incising glacial hanging valleys (Western Alps, France), *J. Geophys. Res.*, *115*, F02010, doi:10.1029/2008JF001079.

1. Introduction

[2] The relative efficiency of glacial, fluvial and hillslope processes operating in orogens remains poorly constrained and improved empirical as well as physically based models are needed [e.g., *Hallet*, 1996; *Whipple et al.*, 2000a] to better constrain the role of surface processes in relief development. During Quaternary times, most mountain belts have experienced glaciations; transitions between glacial and interglacial periods have led to landscape disequilibrium governed by both glacial and fluvial processes. In this context, it appears difficult to assess clearly which processes most strongly control the current transient landforms, as few authors have studied the relative efficacy of glacial versus fluvial erosion [*Whipple et al.*, 1999; *Brocklehurst and Whipple*, 2002; *Montgomery*, 2002; *Naylor and Gabet*, 2007, *Amerson et al.*, 2008; *Koppes and Montgomery*, 2009].

[3] Bedrock gorges are frequent features in fluvial and postglacial landscapes [e.g., *Weissel and Seidl*, 1998; *Crosby and Whipple*, 2006; *Korup and Schlunegger*, 2007], illustrating the potential of fluvial or subglacial erosion in relief evolution. Such gorges are commonly interpreted as transient features [*Schlunegger and Schneider*, 2005]; their origin and evolution can be explained by different processes. Bedrock gorges can be formed by fluvial incision in response to base-level change [*Loget et al.*, 2006; *Harkins et al.*, 2007], multiple climate oscillations leading to transience between glacially and fluvially dominated landscapes [*Schlunegger and Schneider*, 2005], or by subglacial erosion [*Alley et al.*, 2003]. These processes are all active in mountain areas and quantitative landscape analysis is required to identify their relative importance and topographic signatures [*Brocklehurst and Whipple*, 2002] as well as the timing of gorge initiation and evolution.

[4] In this paper, we study bedrock gorges incising glacial hanging valleys in the French Western Alps, with the aim to quantify gorge incision. Hanging valleys are found in many fluvial or glacial contexts and occur at tributary junctions with the trunk valley [e.g., *Anderson et al.*, 2006; *Wobus et al.*, 2006a]. In fluvial landscapes, they occur mainly in actively

[1]Laboratoire de Géodynamique des Chaînes Alpines, Université Joseph Fourier, Grenoble, France.
[2]Géosciences Rennes, Université Rennes 1, CNRS, Rennes, France.

0148-0227/10/2008JF001079

uplifting areas and reflect contrasts in discharge and sediment flux between trunk and tributary channels, although contrasting views have been expressed concerning their formation [*Wobus et al.*, 2006a, *Crosby et al.*, 2007; *Lamb et al.*, 2008a; *Goode and Burbank*, 2009]. In glacial contexts, hanging valleys are explained by the dependence of glacial erosion rates on ice flux (and thus glacial drainage area) and reflect the relative incision capacity between the trunk and tributary glaciers [*MacGregor et al.*, 2000; *Amundson and Iverson*, 2006]. The origin of hanging valleys in the Western Alps is generally considered to be glacial. Steep bedrock gorges incise these hanging valleys, some of which are associated with waterfalls and others with step-pool morphology (as defined by *Montgomery and Buffington* [1997] and *Wohl and Merritt* [2001]).

[5] Both the origin and longevity of such gorges throughout Quaternary times are still poorly constrained. They can be seen as old landscape elements the incision of which was initiated at the beginning of glacial-interglacial cycles; or they may result from postglacial incision [*Valla et al.*, 2009] since ice retreat after the Last Glacial Maximum at ~20 kyr. *Korup and Schlunegger* [2007] have tackled this issue by quantifying the role of bedrock landsliding in inner gorge incision. Their results show strong hillslope-channel coupling during the evolution of inner gorges; these authors conclude that a preglacial origin for at least some of the gorges is plausible, but that postglacial rejuvenation affected most of the gorges. *Valla et al.* [2009] recently reported cosmogenic data that imply Holocene (<10 kyr) incision for a single bedrock gorge (the Diable gorge, also studied here), supporting the hypothesis of a postglacial origin.

[6] Here, we focus on incision processes of fluvial gorges into glacial hanging valleys. Longitudinal profiles of these valleys reveal abrupt breaks in slope (i.e., knickpoints) and well developed oversteepened reaches. The geomorphic setting of these knickzones allows reconstruction of initial knickpoint position and height constraining bedrock incision in response to base-level fall by quantifying knickpoint behavior [e.g., *Bishop et al.*, 2005; *Loget et al.*, 2006; *Harkins et al.*, 2007].

[7] In the following, we characterize fluvial incision of these gorges through morphometric analysis, in particular by studying knickpoint form and valley slope and width adjustments accommodating gorge incision. We then test the ability of different 1-D fluvial incision models to predict present-day gorge profile and channel geometry. Our results suggest that multiple processes are associated with gorge evolution and show that predictions of fluvial incision models should be considered with caution. Finally, we discuss the implications of our results for gorge incision and landscape evolution and review potential research needs to better constrain the origin of these gorges.

2. Study Area

2.1. Geological and Structural Context

[8] We focus on the Ecrins-Pelvoux, Belledonne, Taillefer, and Grandes Rousses massifs, which belong to the "external crystalline massifs" of the French Western Alps (Figure 1). They consist of European crystalline basement blocks that were exhumed along crustal-scale faults [*Ford*, 1996; *Dumont et al.*, 2008] and are separated by remnants of inverted Jurassic extensional basins. The external massifs contain some of the highest peaks in the Alpine orogen, with several summits close to or higher than 4000 m (Figure 1). Although their exhumation started during Oligocene–Early Miocene times [*Leloup et al.*, 2005] several kilometers of denudation have occurred since the Pliocene [*Vernon et al.*, 2008, and references therein] and present-day rock uplift rates reach up to 1 mm yr^{-1} [*Jouanne et al.*, 1995; *Kahle et al.*, 1997]. Several authors have argued that rock uplift may be due to isostatic rebound in response to deglaciation [*Gudmundsson*, 1994] or high erosion rates during Pliocene–Quaternary times [*Cederbom et al.*, 2004; *Champagnac et al.*, 2007]; this question, however, remains debated.

[9] The massifs studied here are bordered by major valleys that separate basement areas from "subalpine" massifs consisting of Mesozoic sedimentary sequences. In our study area, crystalline massifs are limited to the north by the Isère (or Grésivaudan) valley, to the west by the Drac valley, and to the southeast by the Durance valley. The studied massifs are separated from each other by deeply incised valleys (Romanche, Eau d'Olle, and Vénéon), the planform drainage network of which appears to be controlled by structural and lithological trends.

2.2. Geomorphic Setting

[10] Present-day landscape features reveal that the French Western Alps were extensively glaciated during Quaternary times and the landscape is currently affected by efficient postglacial fluvial erosion [e.g., *Brocard et al.*, 2003]. Major valleys (e.g., Grésivaudan and Durance) surrounding the crystalline massifs were occupied by large valley glaciers, which have widened and overdeepened them [*Montjuvent*, 1978]. Glacial overdeepenings were subsequently filled by late glacial and postglacial lake sediments [*Hinderer*, 2001; *Nicoud et al.*, 2002]. Valleys within the major massifs are much narrower but also reflect a strong glacial imprint. Their longitudinal profiles show a succession of characteristic valley steps and flats [*Montjuvent*, 1978] and create a high-relief landscape, with valley bottoms at around ~1000 m and summits over 4000 m elevation. The main trunk valleys show characteristic glacial U shapes for the central part of the Romanche Valley (Bourg d'Oisans trough) and the lower Vénéon and Eau d'Olle valleys. Tributary hanging valleys also show a glacial U-shaped morphology (Figures 2a and 2c) with polished surfaces ("roches moutonnées"). Hanging valley terminations are commonly marked by a bedrock gorge that indicates substantial incision, although smaller hanging tributary valleys may terminate in free-falling waterfalls (Figure 2).

[11] For our morphological analysis, we focused on the Romanche watershed (~1200 km^2) which mainly drains the Ecrins-Pelvoux massif, but also the Taillefer, Grandes Rousses, and Belledonne massifs in its lower part and via its tributaries. The Romanche watershed has been divided into four catchments (Figure 1): Upper Romanche (~360 km^2), Vénéon (~320 km^2), Eau d'Olle (~170 km^2), and Lower Romanche (~350 km^2). The Romanche river, the main river of the region, is ~85 km long and drains all previously cited crystalline massifs before connecting to the Drac river just south of Grenoble. The Vénéon river mainly drains the Ecrins-Pelvoux massif; the glacially overdeepened Bourg d'Oisans trough has formed immediately downstream of its

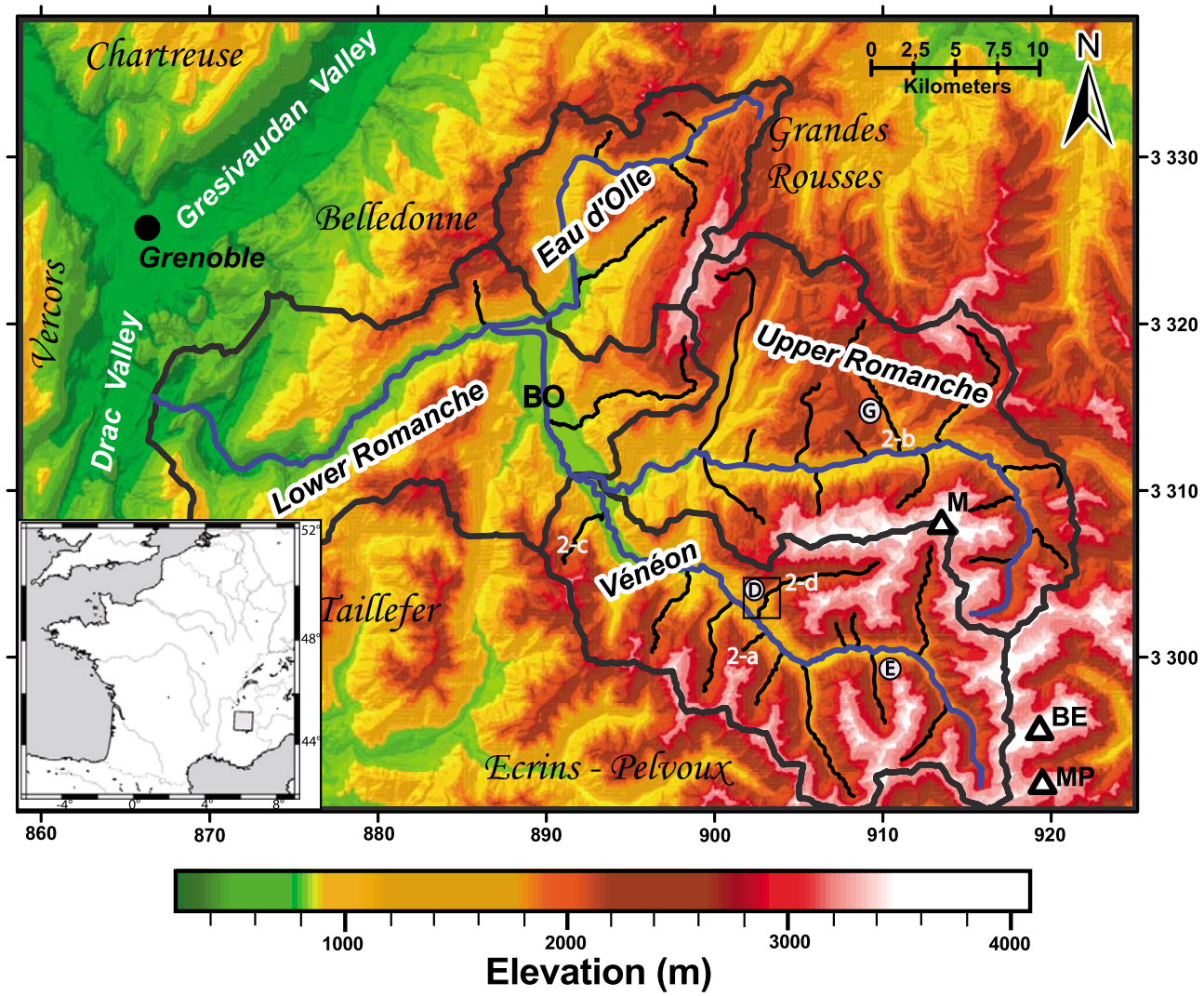

Figure 1. Digital elevation model (Institut Géographique National, 50 m resolution) of the study area showing different major watersheds and selected tributaries, regional massifs, and major summits (M, La Meije (3983 m); BE, Barre des Ecrins (4102 m); MP, Mont Pelvoux (3943 m)). Blue lines are trunk streams; thin black lines are tributary streams with gorges and knickpoints used in this analysis; thick gray lines are catchment boundaries. Locations of views shown in Figure 2 (2a, 2b, 2c, and 2d) and of Diable (D), Etages (E), and Gâ (G) streams are indicated. Small box indicates location of Figure 4b. BO is Bourg d'Oisans glacial trough. Eastings and northings are according to the IGN Lambert-III grid, in kilometers. Inset shows location within France with latitude and longitude.

confluence with the Romanche river. The Eau d'Olle river drains parts of the Belledonne and Grandes Rousses massifs and joins the Romanche river at the northern end of the Bourg d'Oisans trough. Although bedrock gorges also occur in surrounding areas like the Drac watershed, the Gresivaudan valley, or the Vercors and Chartreuse massifs, we restrict our study to the Romanche watershed in order to maintain a homogeneous lithological and geomorphic setting, and thus avoid local complexities, such as differences in tectonic and glacial histories, in our analysis.

3. Data and Methods

[12] We used a 50 m resolution digital elevation model (DEM) acquired from the Institut Géographique National to perform morphometric analyses on the Romanche watershed (Figure 1). First, we extracted the drainage pattern and longitudinal profiles for trunk valleys and their tributaries using TAS [*Lindsay*, 2005] and ArcMap GIS applications. We restricted our analysis to tributaries with characteristic glacial features and with drainage areas >1 km^2 to avoid potential complications for smaller catchments which mainly evolve through processes such as debris flows [e.g., *Stock and Dietrich*, 2003], local mass movements or waterfall erosion. Around thirty gorges were identified, mainly located in the Vénéon and Upper Romanche catchments because these constitute the most elevated parts of the Romanche watershed, but some also occur in the Eau d'Olle and Lower Romanche catchments (Figure 1).

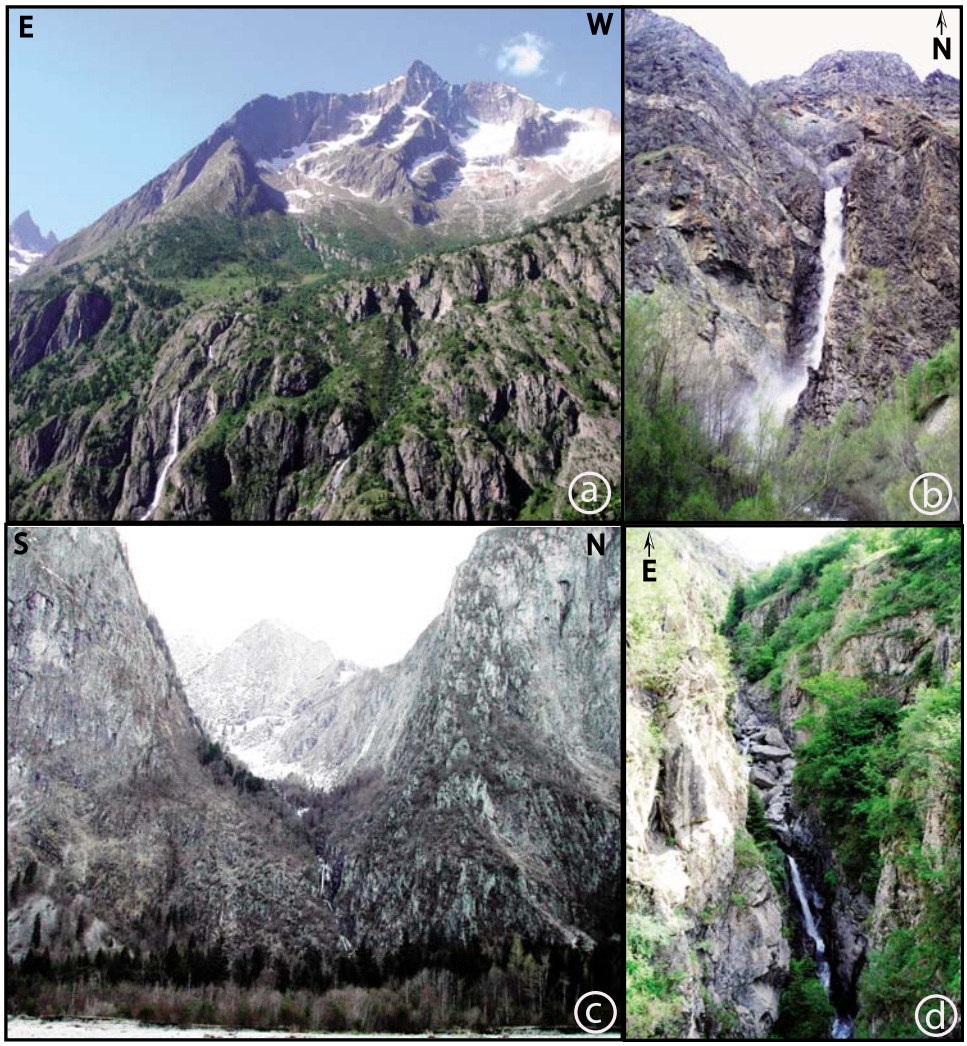

Figure 2. Field photos showing bedrock gorge morphologies (locations in Figure 1). (a) View of a small glaciated catchment with a glacial hanging valley that ends in a waterfall (Cascade de la Pisse, Vénéon valley). (b) Detail of a gorge waterfall incising the sidewall of the trunk glacial valley (Saut de la Pucelle, Gâ gorge, Upper Romanche valley). (c) Confluence between hanging and trunk valley showing incised U-shaped glacial hanging valley form (Vallon stream, Vénéon valley). (d) Bedrock gorge channel, filled with meter-scale blocks, exhibiting step-pool morphology (Diable gorge, Vénéon valley).

[13] We followed several steps to extract morphometric information about gorge morphology. Due to the low resolution of the DEM (50 m) relative to gorge size (typical widths around 10 to 30 m), longitudinal profiles extracted from the DEM contain errors in channel locations and elevations, especially for the gorge location where several cells provide spurious values that strongly overestimate real channel elevations. We tried to correct these errors using topographic maps (10 m contour intervals). Although the maps may contain interpolation errors, smoothing effects are much smaller than for the 50 m DEM; moreover extracted profiles are coherent with our field (handheld GPS) data on channel locations and elevations. River profiles show the same morphological pattern: a concave upper reach with a succession of steps and flats characteristic of a glacially perturbed profile, followed by a convex and steep lower gorge reach (Figure 3). The two reaches are separated by clearly defined knickpoints.

[14] We pinpointed knickpoint locations and oversteepened (gorge) reaches as accurately as possible on each river profile. To achieve this, we used logarithmic slope-distance diagrams for each tributary. Such plots provide similar information as more generally used slope-area plots; however we chose to use this kind of diagram for more direct comparison with the long profiles. Knickpoint locations and total gorge lengths can easily be obtained from this kind of plot [*Brocard et al.*, 2003; *Bishop et al.*, 2005; *Goldrick and Bishop*, 2007]. As an example, Figure 3 shows a slope-distance diagram for the Diable stream in the Vénéon catchment. The gorge reach is not marked by a single knickpoint; rather, the gorge profile shows several knickpoints that mark a well-developed oversteepened reach. We thus identify for each tributary the location of the first major knickpoint, i.e., the beginning of the oversteepened gorge reach (Figure 3). This knickpoint location will be used as the reference for quantifying stream profile evolution during gorge incision,

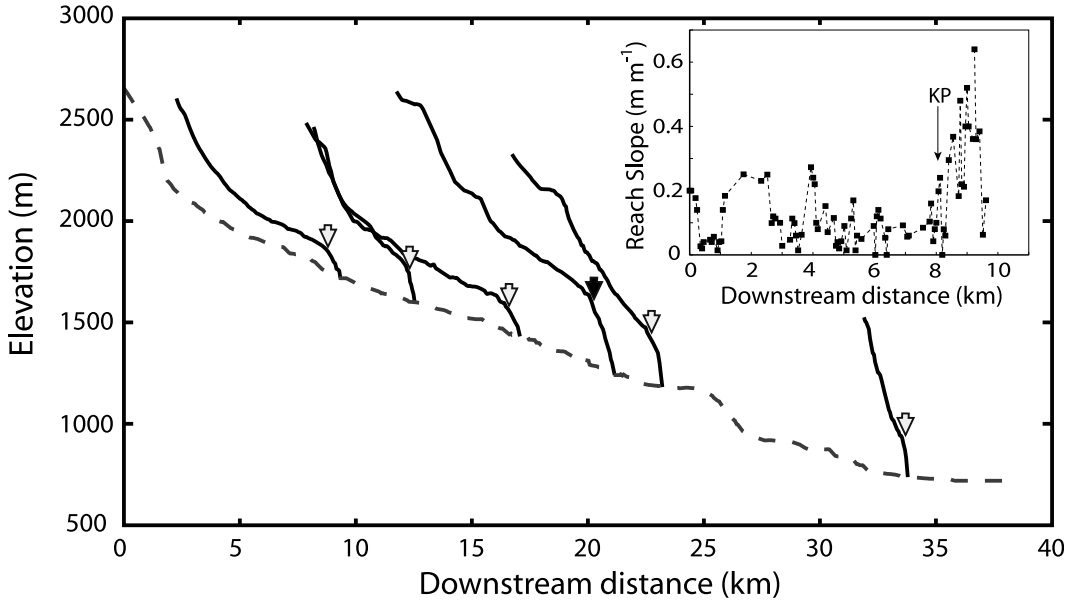

Figure 3. Longitudinal profiles of main tributaries (continuous curves) and the Vénéon trunk stream (dashed curve). Arrows mark locations of knickpoints at upstream ends of gorges. Inset shows slope-distance plot with knickpoint (KP) marking the upper limit of the oversteepened gorge reach for the Diable stream (marked by the black arrow on the main frame).

for which we quantify lateral retreat and potential vertical downwearing of the knickpoint (Figure 4a).

[15] We completed our morphological study with direct channel observations. For three accessible streams (Etages, Diable, and Gâ; see Figure 1 for locations), we measured gorge widths (10–15 measurements) along the stream profile using a laser range distance meter so as to detect possible adjustments in channel geometry accompanying gorge incision [*Duvall et al.*, 2004; *Finnegan et al.*, 2005; *Whittaker et al.*, 2007]. We measured channel width directly both upstream and downstream of the gorge reaches. Access to the gorges themselves was much more difficult due to steep sidewalls. Consequently, most width measurements were performed at the tops of the gorges, except for a few locations along the Diable stream where direct access to the gorge channel was possible.

[16] Potential errors in our measurements need to be considered. For drainage areas, we quantified the perimeter/area ratio for studied watersheds and expect errors to be less than 5%. Profiles contain errors that cannot easily be quantified but may strongly influence our morphometric results and thus our interpretation. We expect errors to be less than ±50 m for horizontal locations (i.e., the DEM resolution). However, elevation errors may be important because grid cells of the DEM are larger than gorge widths and may not fall within the gorge. Expected elevation errors can be quite high (i.e., ±30 m, which can be important compared to gorge depth). Gradient estimates were obtained by different methods. We calculated the mean slope of each gorge by averaging slope along the entire gorge profiles. Local slope estimations were determined for each location where we made channel width measurements. For these estimations, we calculate the finite difference for one DEM cell upstream and downstream of the location and obtained an average value of the local slope. For both slope estimations, we expect errors to be around 20% due to the combined errors in locations and elevations. We made multiple acquisitions for each width measurement and obtained variations less than 0.5 m. Our acquisition method combined with the relatively high resolution of the laser range distance meter lead us to assume maximum errors of ±1 m on width measurements.

[17] For each studied tributary, we reconstructed "initial" profiles that define the landscape before fluvial incision; these are crucial for constraining the initial glacial knickpoint position, and consequently the amount of fluvial incision and knickpoint retreat since gorge initiation. For the upper reach of the tributary, we took the present valley floor as a proxy for the initial profile and extrapolated it by fitting a power law to the profile of the upper reach data. The upper "glacial" reaches generally contain several minor knickpoints; for this

Figure 4. Longitudinal profiles and aerial photograph illustrating reconstruction method for the initial conditions and morphometric data used in our analysis (*d*, knickpoint retreat; *h*, height of tributary valley hang; *i*, knickpoint downwearing). (a) Diable stream profile (open circles and gray dashed curve) and present-day knickpoint (white star) extracted from DEM and topographic map (see Figure 2 for location). Inset shows extrapolated glacial valley floor (black solid curve) obtained by power law fit on "equilibrium" reach immediately upstream of gorge ($Z = 14019\ X^{-0.234}$, $R_2 = 0.995$). Glacial profile end (black squares and gray curve) and initial glacial knickpoint (black star) are also shown. (b) Aerial photograph (Institut Geographique National) of the Diable stream (blue curve) and glacial morphology (red dashed curve) used to reconstruct the initial glacial profile. Black line indicates Vénéon trunk stream. See text for discussion.

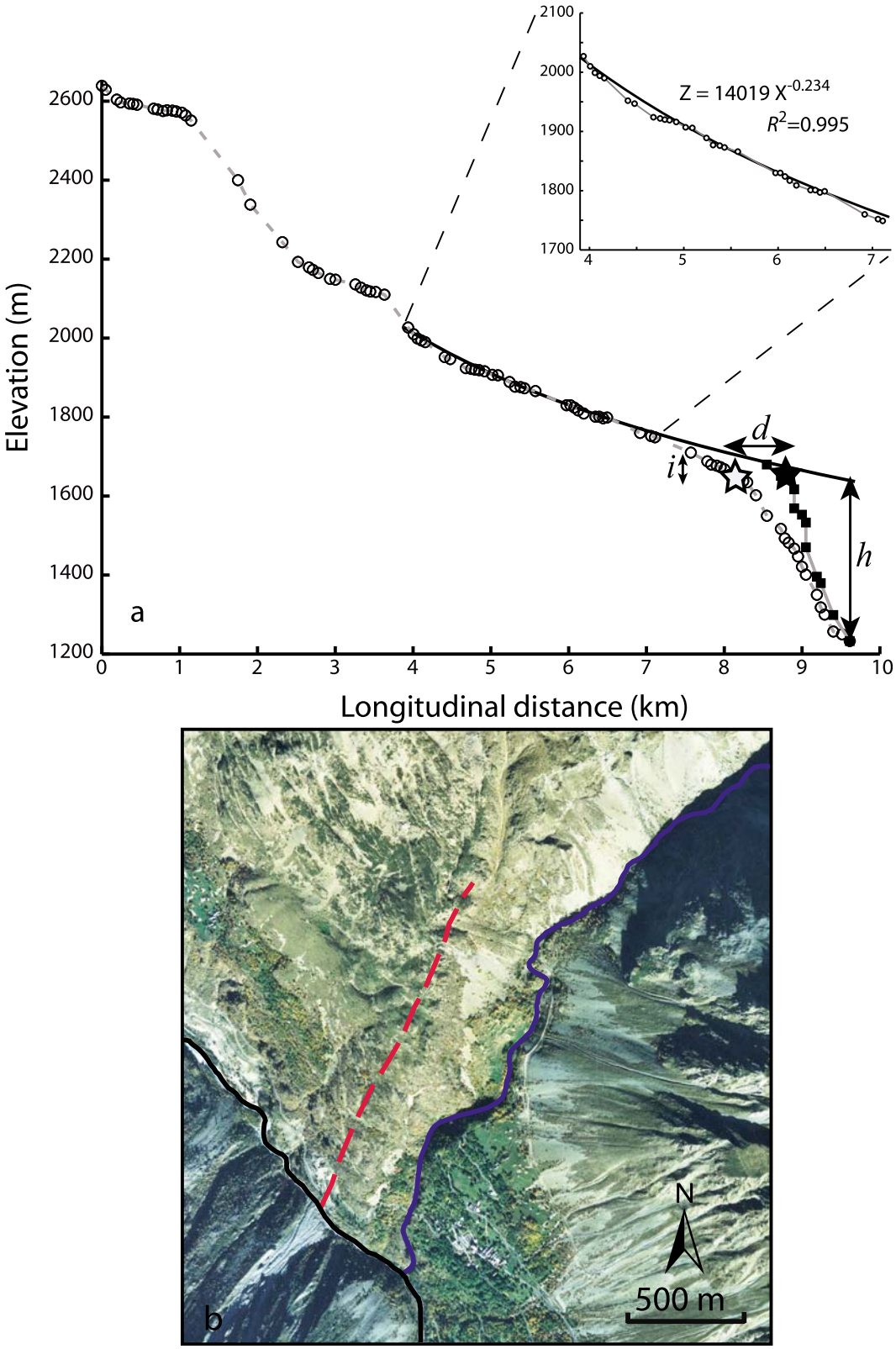
Elevation (m)
Longitudinal distance (km)
Z = 14019 X^-0.234
R^2=0.995
d
i
h
a
b
N
500 m

Figure 4

reason we fitted our power law regression to the first concave reach upstream of the gorge only (Figure 4a). We implicitly assume an "equilibrium" profile for these reaches (several hundred meters to kilometers in length depending the tributary), which may provide an objective proxy for the initial glacial valley floor. Topography close to the gorge has been strongly influenced by gorge deepening and cannot be taken as a reference for the initial glacial profile. Therefore, the downstream ends of the initial profiles were reconstructed using glacially polished bedrock knobs surrounding the gorges (recognized from aerial photographs and field reconnaissance; Figure 4b), assuming that these glacial landforms have not been eroded since the last glacial retreat. The very abrupt break in slope in the glacial profile is in agreement with observed profiles of recently deglaciated hanging tributaries [see, e.g., *MacGregor et al.*, 2000, Figure 1].

[18] These reconstructions assume that trunk stream profiles have not been significantly modified since the last glacier retreat. Trunk streams have typically perturbed transient profiles (see Figure 3) with numerous flats and steps. However, except for some steps where significant incision has occurred, most trunk valleys contain braided streams with an alluvial cover, suggesting they have experienced significant sediment infill (with up to 100 m of sediment thickness in some reaches) since the last glacier retreat. Trunk valley floors currently appear to be mostly characterized by sedimentation and transport. However, without additional geophysical data we are unable to accurately map this sediment infill of trunk valleys except for some locations. Thus, boundary conditions for gorge deepening (i.e., the base level of trunk streams) may have varied by an unknown amount since deglaciation. This may add an error to the determination of the tributary hang height and can also be important for our numerical modeling, as we consider the tributary outlet as fixed (see section 5.2).

4. Morphometric Analysis of Bedrock Gorges

4.1. Knickpoint Origin

[19] We assumed in our introduction that all knickpoints have a glacial origin through the formation of glacial hanging valleys. We based this statement on qualitative field evidence of glacial morphology. Here, we use morphometric analyses to support this inference, by comparing hanging valley heights (i.e., the elevation difference between tributary and trunk valley bottoms) with the contrast in glacial erosion capacity of the trunk and tributary valleys [*MacGregor et al.*, 2000]. Glacial erosion rates are partly controlled by ice discharge [*Anderson et al.*, 2006], which can be approximated to a first order by drainage area [*Amundson and Iverson*, 2006]. We use the reconstructed initial knickpoint elevation with respect to the trunk valley floor as a proxy for the tributary valley hang height. Figure 5 shows that for all catchments (occurring both in sedimentary and crystalline lithologies), tributary hang heights appear to be correlated with the ratio of trunk/tributary drainage areas (all correlations except for Eau d'Olle are statistically significant at the 95% confidence level). This analysis supports the glacial origin of gorge knickpoints. It also suggests that lithology may influence the dependence of hang height on the ratio of drainage areas, as the power law exponent on the hang-height/drainage-area ratio relationship appears to be higher for valleys incising sedimentary rocks (0.36 ± 0.19 (standard deviation) for the Romanche and 0.32 ± 0.10 for the Eau d'Olle, Figure 5b) than for valleys on crystalline basement (0.20 ± 0.07 for the Romanche and 0.23 ± 0.16 for the Vénéon, Figure 5a). Although these ranges overlap because uncertainties in the hang heights are large (±60 m) and the number of data points is relatively low, they provide some support to the notion that glacial erosion is dependent on bedrock resistance [*Harbor*, 1995].

4.2. Bedrock Gorge Channels

[20] Gorges represent highly incised and steep bedrock channels with scarce sediment deposits (see Figures 2b and 2d). In their upper reaches, some channels have an alluvial cover inherited from sediment filling after glacial retreat, but this sediment cover rapidly disappears at the upstream entrance of the gorge. However, meter-scale blocks derived from the gorge sidewalls by major rockfalls are frequent in the channel (see Figure 2d) and may partially protect bedrock from stream incision. Active gorge channels show typical bed morphologies with step-pools, boulder cascades (e.g., Figure 2d), and fluvial abrasion features such as smooth and polished bedrock surfaces, ripples and potholes [e.g., *Whipple et al.*, 2000a]. For gorges incising crystalline lithologies, these morphological features are well developed and remnants of ancient potholes can be seen along gorge sidewalls. Local gorge gradients suggest that bedrock incision can also occur during debris flows [e.g., *Stock and Dietrich*, 2003]. However, field observations suggest that these are not the main process operating as fluvial abrasion forms are preserved in the active channel and debris flow remnants are rare. Finally, amplified erosion due to flow acceleration [*Haviv et al.*, 2006] or waterfall free-fall incision [*Lamb et al.*, 2007] may occur in gorge formation, but free-falling waterfalls currently occur only at the outlet of the smallest tributaries, where the glacial knickpoint has hardly retreated because the upstream drainage area is quite small. We thus suggest that this process might be restricted to the early stages of the gorge incision or to small tributaries.

[21] Because the studied gorges are located at the confluence between glacial hanging and trunk valleys, the gorge morphology can be influenced by either trunk or tributary valley dynamics such as fluvial aggradation/incision or slope processes. Figure 6 shows that, although we study tributaries from different catchments, there is a clear correlation between tributary drainage area and mean gorge gradient; hanging valleys with large drainage areas exhibit gentler averaged gorge gradients than smaller tributaries (the correlations are significant at the 95% confidence level). In contrast, we do not find any correlation between trunk drainage area and gorge gradient, which suggests that mean gorge gradients do not show any influence of the trunk valley; however, they reflect the greater erosional capacity of larger tributaries [*Wobus et al.*, 2006a]. Figure 6 also shows lithological effects on gorge gradient; although all gorges follow the same inverse correlation between mean gradient and tributary drainage area (the power law exponent is -0.40 ± 0.14 for crystalline lithologies and -0.41 ± 0.15 for sedimentary rocks), gorges incising sedimentary rocks have lower mean slopes than those in crystalline basement for similar upstream drainage area. This observation might suggest that gorge gradients are modulated by lithology, although this difference

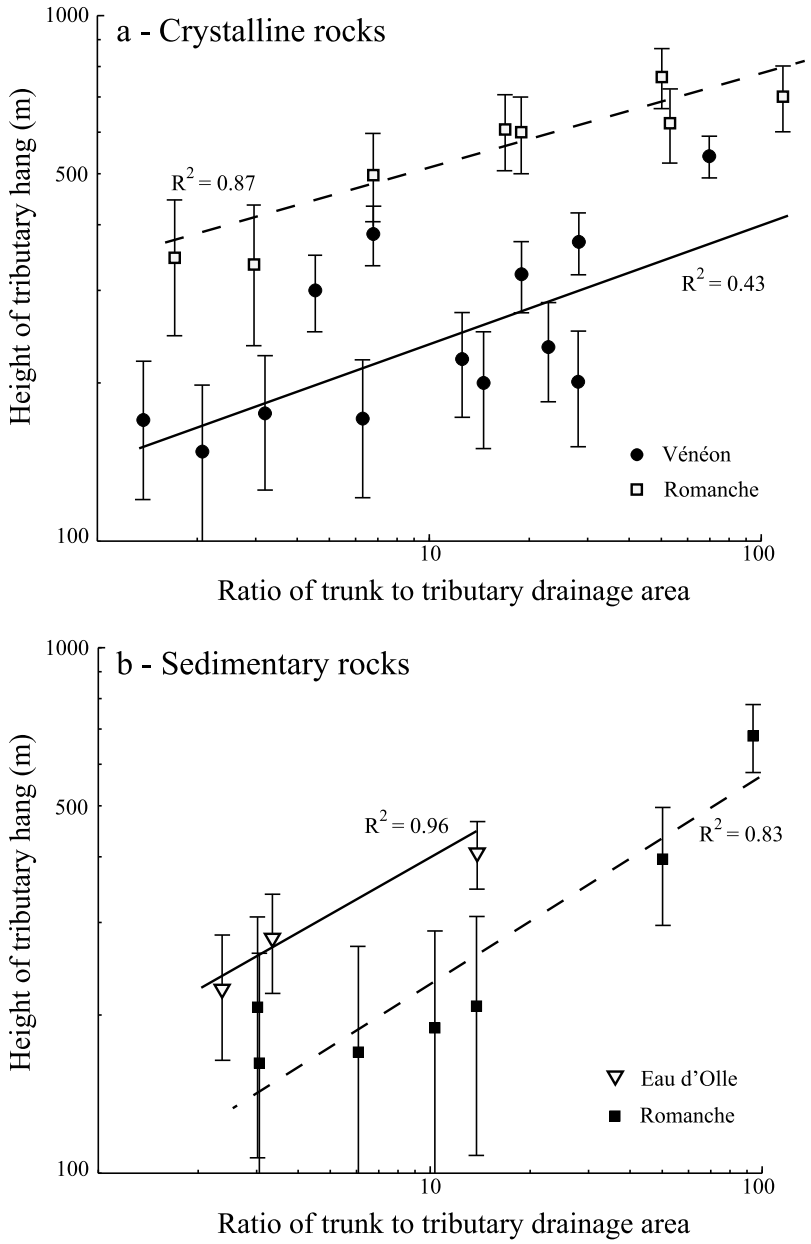

Figure 5. Logarithmic plot showing height of tributary valley hang as a function of ratio of tributary to trunk drainage area for (a) tributaries on crystalline basement (power law exponent of 0.20 ± 0.07 for Romanche and 0.23 ± 0.16 for Vénéon) and (b) tributaries draining sedimentary lithologies (power law exponent of 0.36 ± 0.19 for Romanche; 0.32 ± 0.10 for Eau d'Olle). Errors on tributary heights (±60 m) are indicated.

is not statistically significant as the two data sets overlap. The link between gorge gradient and trunk drainage area may also reflect conditions inherited from glaciations during which larger tributaries acquired smaller hang height because of more similar glacial erosion with the trunk valley. This difference may have been enhanced by postglacial fluvial processes since deglaciation, the larger tributaries reflecting faster knickpoint retreat than smaller ones (see section 4.3 and Figure 8).

[22] Measured local width variations (Etages, Diable, and Gâ, Figure 7) indicate an inverse correlation between channel widths and estimated local slopes. For all three streams, largest widths were encountered in the upstream reaches of the profiles (the glacial valley floor), characterized by very gentle slopes (<0.01 m m^{-1}). Here, the streams incise fluvioglacial sediments and braid across the valley floor. When entering the gorges, the streams start incising bedrock; channel widths are greatly reduced (up to 10 times) and are associated with higher slopes. Width measurements were easier for the upper reaches of the profiles because channel banks are clearly marked by sediment terraces in these reaches. Measurements within the gorge were much more difficult to make, as previously discussed. When measuring gorge width from the top of the gorges, we assume that active

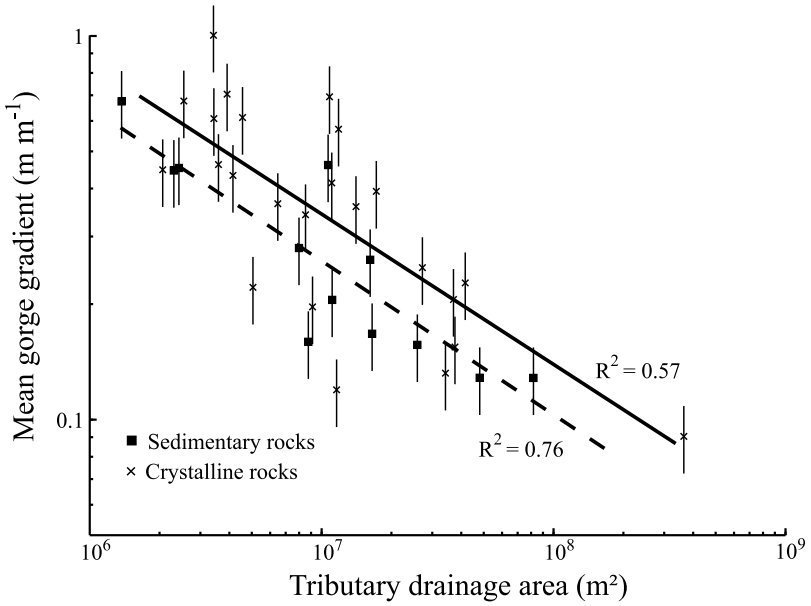

Figure 6. Logarithmic plot showing the relation between mean gorge gradient and tributary drainage area. Note that for similar drainage areas crystalline lithologies (crosses and black curve) present higher gradients than sedimentary lithologies (squares and dashed curve) even though the slope exponent of the correlation is the same (crystalline, -0.40 ± 0.14; sedimentary, -0.41 ± 0.15). Errors of ±20% for averaged gorge slope are indicated.

channel widths are close to the top widths, i.e., gorge sidewalls are close to vertical and the channel fills the gorge floor. Keeping these methodological limitations in mind, we show that the three streams exhibit the same trend between local slope and channel width (Figure 7). Moreover, the data suggests that regression slopes are modulated by drainage area. For the Etages, which is the smallest basin (14 km^2), the slope coefficient is higher in absolute value (1.23 ± 0.36) than for the Diable (0.59 ± 0.21) and the Gâ (0.23 ± 0.09), which have larger drainage areas (20 and 42 km^2, respectively).

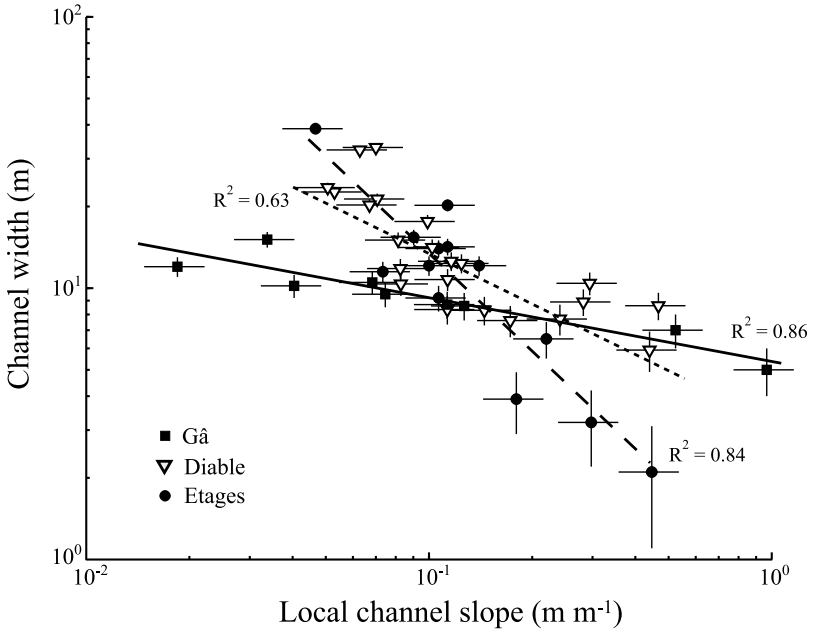

Figure 7. Channel width and slope variations (logarithmic plot) for the Etages (circles and dashed curve), Diable (inverted triangles and dot curve), and Gâ (squares and solid curve) streams. Note that the exponent of the power law correlation between local gradient and channel width (Etages, -1.23 ± 0.36; Diable, -0.59 ± 0.21; Gâ, -0.23 ± 0.09) appears to be modulated by tributary drainage area (Etages, 14 km^2; Diable, 20 km^2; Gâ, 42 km^2). Errors on slope (±20%) and width (±1 m) values are indicated.

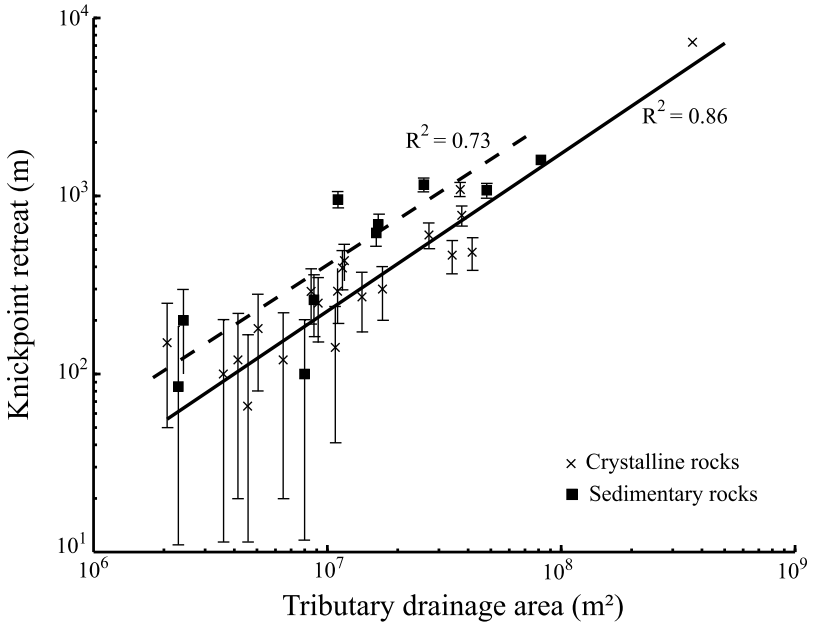

Figure 8. Logarithmic plot of knickpoint retreat versus tributary drainage area for all selected gorges. Note that for similar drainage areas, knickpoint retreat is less in crystalline lithologies (crosses and solid curve) than in sedimentary lithologies (squares and dashed curve), even though the exponent of the power law correlation is the same (crystalline, 0.83 ± 0.17; sedimentary, 0.79 ± 0.39). Single very large catchment (2×10^8 m^2) is upper Romanche river and Infernet gorge upstream of junction with Vénéon (compare Figure 1). Errors on knickpoint retreat (±100 m) are indicated.

Channel width thus appears to be both influenced by local slope variations and dependent on the stream discharge, illustrating dynamic channel evolution along the gorge to sustain incision [*Finnegan et al.*, 2005; *Wobus et al.*, 2006b]. We suggest that these channel adaptations accompanying fluvial incision have strong implications for water and sediment flow through the gorge and thus have consequences for gorge deepening.

4.3. Knickpoint Distribution and Characteristics

[23] Knickpoint evolution can operate through different ways depending on climatic and tectonic context or basement lithology (see *Gardner* [1983] and *Frankel et al.* [2007] for detailed discussions). In our introduction, we have assumed coeval knickpoint evolution for all studied tributaries, i.e., that glacial retreat has been rapid and synchronous on the scale of the Romanche watershed. Here, we interpret knickpoint evolution to start from an abrupt glacial knickpoint that wears back by fluvial processes (Figure 4a). Our morphometric analysis indicates that both vertical downwearing and horizontal retreat of knickpoints take place during gorge incision. The amount of knickpoint retreat is correlated with tributary drainage area (Figure 8). This dependence has been described in other fluvial settings [*Hayakawa and Matsukura*, 2003; *Bishop et al.*, 2005; *Crosby and Whipple*, 2006; *Berlin and Anderson*, 2007; *Lamb et al.*, 2007] and is consistent with fluvial incision models in which incision and knickpoint retreat rates are dependent on drainage area [e.g., *Whipple and Tucker*, 1999]. The relationships shown in Figure 8 also suggest that the regression slope is the same for sedimentary and crystalline lithologies (0.83 ± 0.17 for crystalline basement and 0.79 ± 0.39 for sedimentary rocks). Moreover, assuming a coeval knickpoint evolution, it appears that knickpoint retreat rates are higher in sedimentary lithologies than in crystalline rocks for similar drainage areas (Figure 8); this difference is statistically significant at the 95% confidence level.

[24] As previously noted, vertical downwearing of knickpoints is more ambiguous due to large errors on elevations (see section 3) and cannot be directly related to parameters describing either the trunk or the tributary valleys (Figures 9a and 9b). We suggest that this absence of correlation for vertical knickpoint evolution is due to two opposing controls: the initial knickpoint is higher for smaller tributaries (larger ratio of trunk/tributary drainage areas) but the erosion capacity of the tributary stream is higher for larger drainage areas. Moreover, no correlation is observed between vertical downwearing and horizontal retreat of knickpoints (Figure 9c). *Niemann et al.* [2001] suggested that knickpoint elevations may be comparable for tributaries experiencing the same wave of incision from the trunk stream [*Harkins et al.*, 2007]. However, this is not the case for hanging valleys where gorge incision occurs in response to both the relative height difference between tributary and trunk streams and the tributary drainage area; we thus suggest that in these settings knickpoint elevation and its evolution cannot be used directly to quantify processes associated with gorge deepening [*Wobus et al.*, 2006a].

5. Constraints From Fluvial Incision Modeling

[25] In this section, we employ 1-D numerical modeling to test different fluvial erosion algorithms for gorge incision. We do not exhaustively review all existing fluvial incision models because this has already been done by several authors

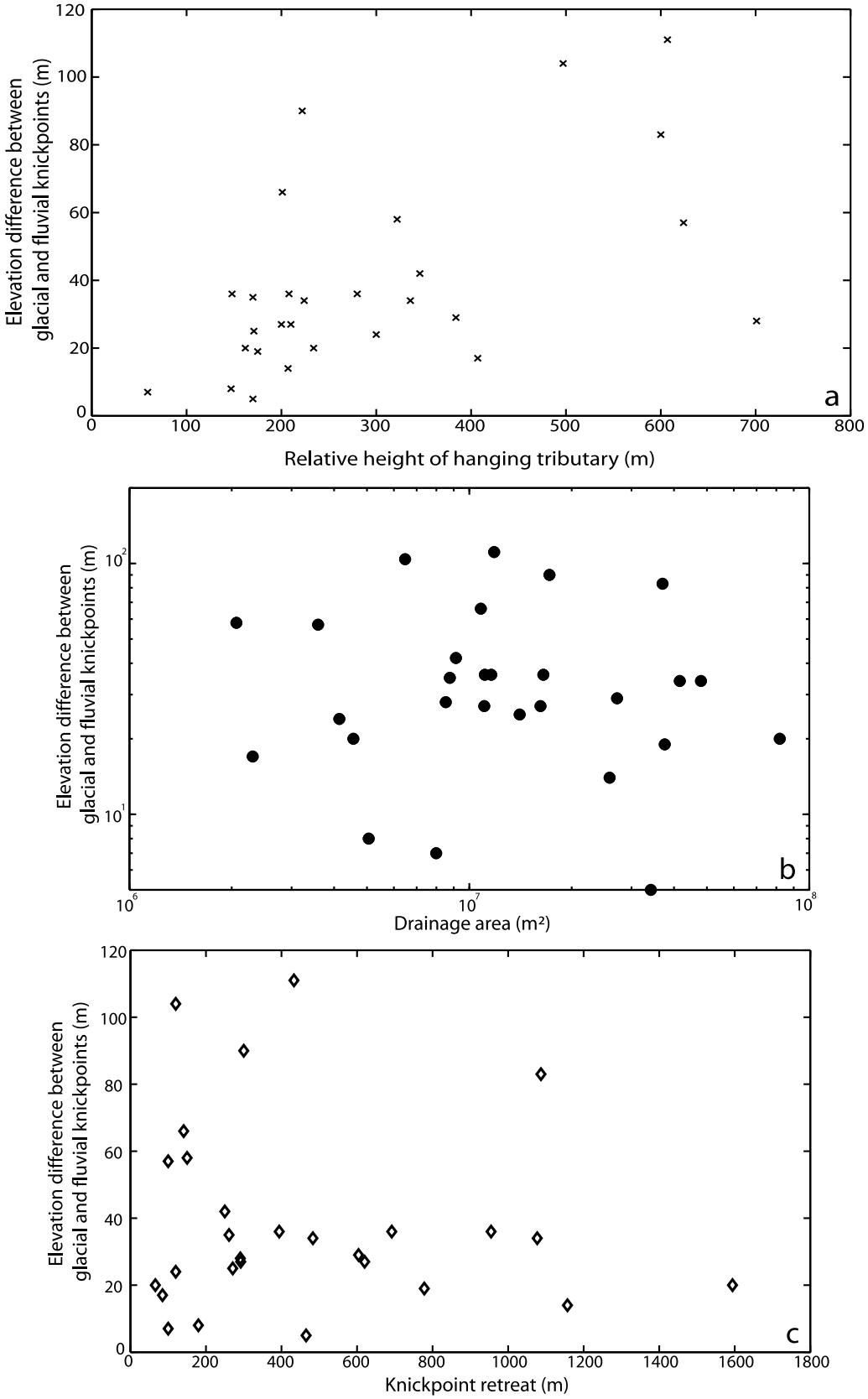

Figure 9. Vertical lowering of tributary knickpoints versus (a) height of the tributary hang, (b) tributary drainage area, and (c) knickpoint retreat. No clear correlations appear (see text for discussion). Note that elevation differences are between 0 and 120 m and thus relatively close to data resolution (±30 m).

[e.g., *Tomkin et al.*, 2003; *van der Beek and Bishop*, 2003]; we instead focus our study on three formulations that describe different processes for bedrock incision.

5.1. Fluvial Incision Models

[26] Fluvial incision algorithms abound in the literature and are widely used for landscape evolution modeling. The most general models are based on the hypothesis that incision rate should be proportional to either total stream power, unit stream power, or basal shear stress [*Howard et al.*, 1994; *Whipple and Tucker*, 1999]. These formulations can be written using slope and drainage area power laws as proxies for stream power, leading to the well-known "stream power law" for fluvial incision:

$$\dot{E} = K A^m S^n \tag{1}$$

where $\dot{E}$ is fluvial incision rate (m yr^{-1}), K is a dimensional constant reflecting the resistance of the substrate to incision (m$^{(1-2m)}$ yr^{-1}), S is local stream gradient (m m^{-1}), A is drainage area (m^2), and n and m are dimensionless exponents supposedly reflecting the physics behind the models (for further details, see *van der Beek and Bishop* [2003]), but possibly dependent on other factors such as discharge variability [*Lague et al.*, 2005]. For these models, width variations are assumed to be dependent on drainage area only ($W \sim A^{0.5}$) and are consequently implicitly incorporated in the incision algorithm. In their simplest form, stream power law models do not take into account sediment transport; bedrock incision rates are only limited by the stream power of the river and they are referred to as "detachment-limited" models (see *Whipple and Tucker* [2002] for a discussion).

[27] An alternative formulation for fluvial incision argues that bedrock incision rates could be limited by the river's capacity to transport and export eroded materials [e.g., *Willgoose et al.*, 1991; *Tucker and Whipple*, 2002]. Such "transport-limited" models take sediments into account as a limiting factor for bedrock incision because stream power is expended in sediment transport. These models are based on the transport capacity Q_{eq} of the river, which is taken as a function of stream power:

$$Q_{\mathrm{eq}} = K_s A^{m_s} S^{n_s} \tag{2}$$

where again K_s is a dimensional constant (m$^{(3-2m_s)}$ yr^{-1}) and n_s and m_s are dimensionless exponents. This formulation assumes that the river is always at carrying capacity; spatial variations in the carrying capacity lead to incision or deposition. Incision rates are thus calculated by combining equation (2) with the following continuity equation:

$$\dot{E} = \frac{1}{W}\frac{\delta Q_s}{\delta \vec{x}}; Q_s = Q_{eq} \tag{3}$$

where $\vec{x}$ is the flow direction and W the channel width (m). Unlike detachment-limited models, transport-limited models may take width variations and sediment transport along the stream explicitly into account. In our modeling, we include width variations by assuming that the slope-width relation currently observed along the gorge (Figure 7) is valid during the entire episode of gorge deepening.

[28] Although the detachment- and transport-limited models are most generally used for landscape evolution modeling [e.g., *Anderson*, 1994; *Willett*, 1999], they ignore several potentially important controls on fluvial incision, including thresholds and stochastic distributions of discharge [e.g., *Tucker*, 2004, *Lague et al.*, 2005], dynamic adaptation of channel geometry [e.g., *Finnegan et al.*, 2005; *Turowski et al.*, 2006; *Wobus et al.*, 2006b] and the interaction between sediment and bedrock [e.g., *Sklar and Dietrich*, 1998, 2006; *Johnson et al.*, 2009]. Sediment supply and transport by the river can influence bedrock incision in two different ways: at low sediment fluxes, sediments impact the bedrock, providing efficient "tools" for erosion and increasing the incision capacity of the stream; large amounts of sediments, in contrast, partially cover and protect the bed from erosion [e.g., *Sklar and Dietrich*, 2004]. We investigate these potential controls by using a new fluvial incision algorithm described extensively by *Lague* [2010]. As opposed to the simple end-member detachment- and transport-limited models, this model factors in various elements of the complexity of bedrock incision, including a stochastic variation of discharge and sediment flux at daily time scales, a separate calculation of bed and bank incision rate allowing width and slope to vary dynamically, and tracking of sediment transport and deposition in the channel to compute static and/or dynamic cover effects. Our objective in using this model is not to deliver a perfectly calibrated set of parameters, but rather to show the effect of taking into account these important but ill-understood controls on stream incision. As discussed by *Lague* [2010], many elementary ingredients of the numerical model are still only partially understood or are built on empirically derived laws (hydraulics, sediment transport, incision laws, mode and timing of sediment supply from hillslopes…). Yet, even with these limitations, we show that only a limited set of conditions of hillslope/channel coupling lead to the present-day profile geometry (slope, width and sediment thickness). We summarize the main features of the numerical model (referred to in the following as the "cover" model) and the boundary conditions used for gorge incision modeling in Appendix A. Details of the numerical procedure and the justification of chosen elementary laws of incision and transport are given by *Lague* [2010].

[29] In the following, we assess these three different models in terms of their capability of adequately reproducing the present-day river longitudinal profiles and channel geometry of the studied gorges.

5.2. Modeling Approach

[30] We model three tributary streams (Diable, Etages, and Gâ) for which we have both profile and width data. The starting condition for all numerical simulations is given by the reconstructed initial profile (see Figure 4a); the present fluvial profile is taken as a reference to test the ability of our models to predict present-day gorge geometry. Both profiles are linearly interpolated to a uniform 5 m horizontal spacing. The variation of drainage area along the stream profiles is included using Hack's law ($A \sim k X^a$, where A is drainage area, X is distance from the divide, and k and a are fit constants). The fit constants in Hack's law were estimated for each stream using TAS [*Lindsay*, 2005]. This method assumes that the tributary drainage pattern has not changed since gorge initiation; this assumption seems reasonable for these relatively small valleys that are delimited by high ridges and that are not joined by tributaries within the gorge.

[31] For the transport-limited model, channel widths evolve through the width/slope relationship that was deduced from field observations (Figure 7); whereas in the cover model, the evolution of channel width is a model prediction for which initial conditions are those measured in the field just upstream of the gorge, assuming that they are proxies for the immediate postglacial channel widths. Best fit values for the controlling detachment-limited (K, n, and m) and transport-limited (K_s, n_s, and m_s) models are searched by comparing predicted and observed fluvial profiles. In the cover model, the parameters K_{ref}, K_{bank}, K_{sed}, ξ, ν, and Q_{wall} are set as free parameters during our modeling. Detachment- and transport-limited models are thus three-parameter models, whereas the cover model is a two-parameter model for calculating incision (K_{ref}, K_{bank}) when sediment effects are neglected, but for which we add four more degrees of freedom for sediment supply (from gorge sidewalls and surrounding hillslopes) and transport. Note however, that we have additional constraints for the cover model compared to the detachment- and transport-limited models, which only consider channel profile: cover model predictions compared to observed data include along-stream channel width and mean sediment thickness on the bed.

[32] Numerical simulations are achieved by integrating the fluvial incision algorithms through time using a finite difference technique with adaptive time stepping [*Press et al.*, 1992] for the detachment- and transport-limited models, and constant time step of 1 day for the cover model. The downstream boundary condition was fixed at the elevation of the tributary junction with the trunk stream throughout the model run. As discussed in section 3, this is a simplification as the trunk valleys may have been glacially overdeepened and filled by an unknown amount of postglacial sediment. However, at all three tributary junctions, the trunk valley is relatively narrow and bedrock is widely exposed (compare Figure 4b for the Diable example). We thus believe that the fixed base-level assumption does not introduce major errors into our analysis. We assume for numerical modeling that bedrock gorges are purely post-LGM features based on recent cosmogenic data for one gorge [*Valla et al.*, 2009]; all models are run for 20 kyr, which is a rough estimate for the onset of glacial retreat in the Alps [*Hinderer*, 2001; *Ivy-Ochs et al.*, 2004]. However, the exact timing of onset of gorge incision is not critical for our simulations, as incision rates are linearly dependent on a dimensional constant in all models (K, K_s, or K_{bank}/K$_{ref}$). Varying these constants leads to exactly the same evolution of the gorges but at a different rate, except for the cover model where incision is more complex due to the incision threshold and sediment cover effect. We test model performance by calculating the root-mean-square (RMS) deviation between predicted and observed fluvial profile elevation (and thus stream incision) at the end of the simulations:

$$RMS = \sqrt{\frac{\sum_{i=1}^{n} \left(h_{obs,i} - h_{\mathrm{mod},i}\right)^2}{n}} \quad (4)$$

where n is the number of data along the profiles and h_{obs} and h_{mod} are observed and modeled present-day streambed elevations, respectively. A parameter search was performed for all models through a systematic trial-and-error process.

5.3. Model Results and Implications for Gorge Dynamics

[33] We first report results for the stream power models as they constitute simple end-member fluvial incision laws before presenting modeling results for the cover model. For each model, we ran numerous trial-and-error simulations to constrain acceptable values of m and n (or m_s and n_s). For the detachment-limited model, m and n values characteristic for abrasion processes can be found in the literature [*Whipple et al.*, 2000a] and are expected to depend on the physical theory of the stream power law (see *van der Beek and Bishop* [2003] for more details). We thus chose to restrict m and n variations between [0.3;1.0] and [0.7;1.0], respectively, which are the most common values for stream power models, although some studies [e.g., *Stock and Montgomery*, 1999; *Kirby and Whipple*, 2001] have come up with m and n ranges that were much larger than theoretical predictions. The exponents m_s and n_s for the transport limited model are more difficult to constrain and for simplicity many studies have chosen unity values for m_s and n_s [e.g., *Kooi and Beaumont*, 1996]. Following previous studies [*van der Beek and Bishop*, 2003], we chose to vary m_s and n_s between [1.0;1.3] and [0.4;1.0], respectively.

[34] Although we tested several m and n combinations, differences between various m/n values are small (Figure 10a) and relatively small misfits are found for values close to unity ($m = n = 1$). This unusual result (when compared, for instance, to *Stock and Montgomery* [1999], *Tomkin et al.* [2003], or *van der Beek and Bishop* [2003]) can be attributed to the specific evolution of channel width, which decreases downstream in the gorges. We thus report results for the linear stream power model in Figure 10. Values for K range between 5 and 7 $\times$ 10^{-10} m^{-1} yr^{-1} for the three rivers; even best fit models, however, retain high RMS misfit values (41 m for Diable, 23 m for Etages and 30 m for Gâ; compare Figure 10). Linear detachment-limited models predict parallel retreat of knickpoints without downwearing or any diffusive component [e.g., *Howard et al.*, 1994]. Some studies [e.g., *Tucker and Whipple*, 2002] have modeled diffusive profile steps using values of $n < 1$. We tested these conditions for the three rivers; although we managed to predict some knickpoint lip diffusion, RMS misfit values are comparable to the linear model. These results are explained by the mostly advective behavior of the knickpoint, which leads to excess incision of the lower profile reach (Figures 10 and 12). Detachment limited conditions thus do not predict the observed evolution of glacial knickpoints by "replacement" [*Gardner*, 1983; *Frankel et al.*, 2007], highlighting their inability to predict long-term fluvial dynamics of gorge deepening in our specific case.

[35] We adopt the same approach for the transport-limited model; again m_s and n_s variations provide best fit results

Figure 10. Initial glacial (squares) and present-day fluvial (circles) profiles for (a) Diable, (b) Etages, and (c) Gâ streams, and profile evolution predicted by the best fit detachment-limited model ($m = n = 1$; K as indicated in the plots). Thick lines show profiles at 5 kyr intervals during the model run (dotted, 5 kyr; dashed-dotted, 10 kyr; dashed, 15 kyr; solid, 20 kyr). Inset in Figure 10a shows dependence of predicted present-day profile on choice of m and n exponents.

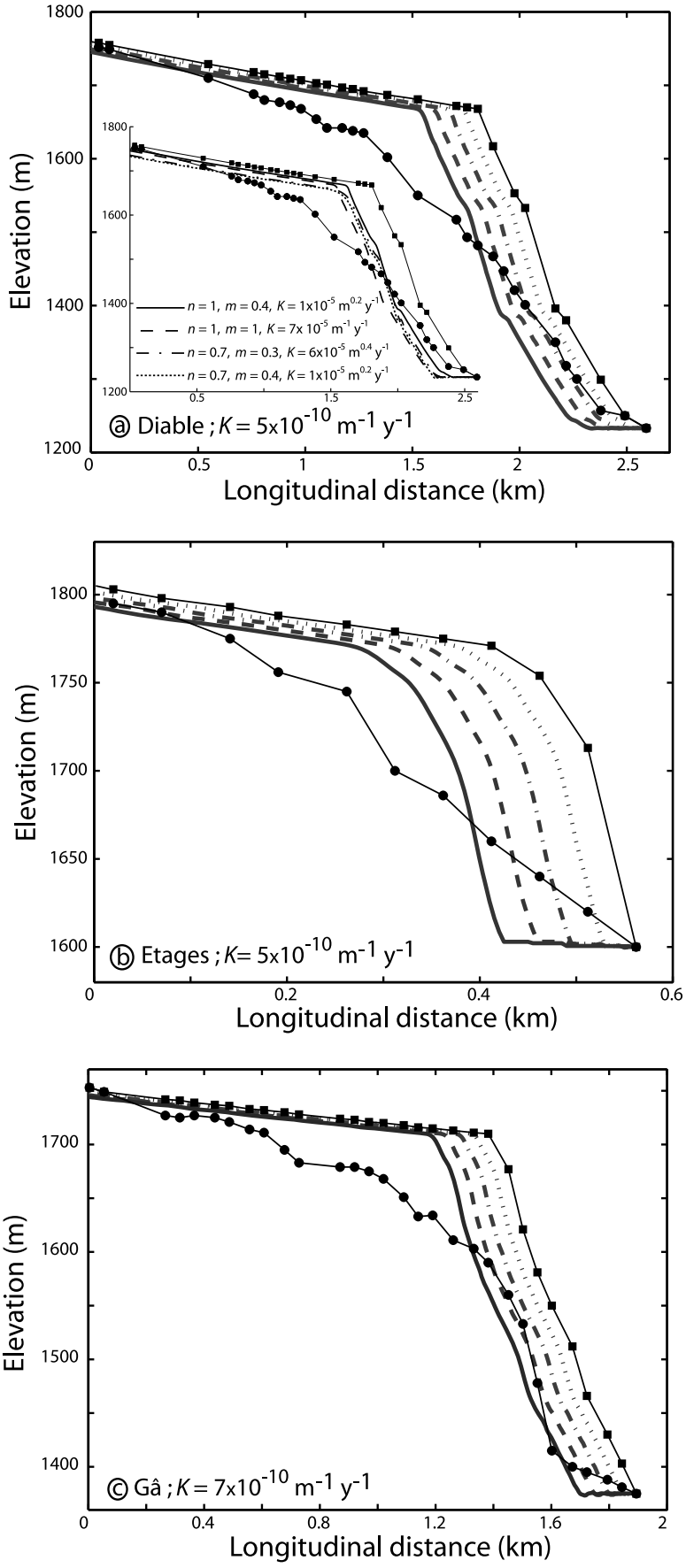
Elevation (m)
Longitudinal distance (km)
n = 1, m = 0.4, K = 1x10-5 m0.2 y-1
n = 1, m = 1, K = 7x 10-5 m-1 y-1
n = 0.7, m = 0.3, K = 6x10-5 m0.4 y-1
n = 0.7, m = 0.4, K = 1x10-5 m0.2 y-1
ⓐ Diable ; K = 5x10-10 m-1 y-1
ⓑ Etages ; K= 5x10-10 m-1 y-1
ⓒ Gâ ; K = 7x10-10 m-1 y-1

Figure 10

for the linear model, with K_s values ranging from 2×10^{-6} to 3×10^{-5} m yr^{-1}. Transport-limited simulations, including explicit width variations in space and time, provide much better fits (RMS misfits of 14 m for Diable, 4 m for Etages and 20 m for Gâ) between predicted and observed profiles (Figure 11) than the detachment-limited model. This is mainly because the transport-limited algorithm includes a diffusive component in the incision formulation; numerical simulations thus reproduce knickpoint evolution by replacement. The difference between the two models shows up most clearly when looking at the distribution of incision along the longitudinal profiles (Figure 12). Although both models correctly reproduce fluvial deepening for the most upstream part of the profile, detachment-limited models strongly underestimate knickzone incision and overestimate fluvial incision for lowest part of the profiles due to the strong advective component of these models. In contrast, transport-limited models provide realistic predictions of gorge incision except for the lowest profile reach. We believe the misfit in this reach may be due to efficient sediment entrainment in this area resulting from interactions with the trunk stream, as well as potential transient base-level effects, which are both not included in our models.

[36] These initial results show that transport-limited models provide much better predictions for stream profile evolution in these gorges than detachment-limited models. This outcome is surprising in the light of field indications for present-day incision dynamics: the gorge walls and floor show smooth polished bedrock surfaces characteristic of incision by abrasion and plucking in a detachment-limited setting [*Whipple et al.*, 2000a]. Moreover, except for meter-scale blocks in some reaches, sediment deposits are scarce along the gorges and sediment transport does not appear to be the limiting incision process during recent times.

[37] The above paradox between the morphological evidence for current gorge dynamics and the long-term numerical predictions for stream-profile evolution suggests that simple end-member models may not be appropriate to model gorge evolution, or that the field evidence pertains only to present-day channel conditions. We therefore attempt to model gorge evolution using the more elaborate cover model. However, this model requires more information about stream dynamics and sediments (bank angle, $D_{50,}$ bed load proportion, mean discharge and discharge variability, see Table 1) than the end-member models. We did not have access to the active channel of the Gâ and Etages gorges and thus could not estimate these parameters. Moreover, initial results with end-members models indicate that the Diable, Etages, and Gâ streams are governed by similar long-term dynamics as K or K_s values are similar for the three streams (even if the nature and importance of incision processes might be different in the three gorges). Thus, we decided to limit simulations using the cover model to the Diable stream, because this is the only gorge for which we managed to estimate the channel morphology and sediment properties.

[38] Initial runs with the cover model do not include a dependence of incision rate on sediment cover, as we wanted to first verify the ability of a more realistic detachment-limited model, including an incision threshold, stochastic discharge distribution and dynamic width adjustment, to predict gorge deepening. We constrain the K_{ref} and K_{bank} parameters, which are the key for setting gorge incision. If bank erosion is too low compared to bed erosion, gorge incision will be extremely efficient and will lead to very narrow and deep channels. On the contrary, if bank erosion is too high compared with bed erosion, the gorge channel will widen and consequently decrease shear stress and incision of its bed. These two incision parameters thus have to be correctly adjusted to predict realistic present-day stream profiles and channel widths that match the field and morphometric observations.

[39] Best fit runs for the model without the cover effect predict widths of 20–25 m and gentle slopes (0 to 0.01 m m^{-1}) above the knickpoint and close to the confluence with the trunk valley, contrasting to narrow predicted widths (5–10 m, Figure 13a) and high slopes (0.25 to 1 m m^{-1}) for the gorge reach. These results compare favorably to measured values for the Diable gorge (see Figures 7 and 13a). However, numerical simulations lead to a relatively high misfit between predicted and observed stream profiles; the RMS misfit of ~25 m is much lower than the basic detachment-limited model but is still larger than results from transport-limited models (Figure 13a). In essence, the behavior remains mostly advective, with parallel retreat of the gorge. The downstream part of the gorge is less steep than in the detachment-limited model because of the inclusion of a critical threshold of incision. Thus, taking into account spatial and temporal variations in channel geometry and a realistic discharge distribution combined with a threshold of erosion has improved numerical predictions of gorge incision, even though this appears not to be sufficient to predict gorge deepening with a simple detachment-limited formulation.

[40] When sediment effects are taken into account, if the transport capacity (Q_{eq}, which depends on K_{sed} parameter) of the channel is too high, or the sediment supply (q_{lat}, which depends on Q_{wall} parameter) too low, the sediment does not significantly limit downstream of knickpoint incision, and the profile evolution is similar to the detachment-limited models. On the contrary, if the sediment supply is too large with respect to transport capacity, the channel is rapidly filled with sediment and cannot incise vertically anymore. Hence, as the present-day channel does not have a significant cover of sediment (less than 1 m in the gorge, even though this is a value largely variable in time and not representative of long-term values) [*Lague*, 2010], this places an upper boundary on the ratio q_{lat}/Q_{eq} above which the model predicts too much sediment deposited in the channel. A large q_{lat} would also imply extremely rapid erosion of the gorge sidewalls and hillslopes. We found that a value of $Q_{wall} \sim 9$ mm yr^{-1}, combined with a value of $K_{sed} = 1.4\ 10^{-7}$ m$^{5/2}$ s^2 kg$^{-3/2}$ provided realistic predictions of mean sediment thickness in the gorge (see Table 1 and Appendix A for details). This would suggest an erosion of the gorge sidewall and surrounding hillslopes of ~180 m since the LGM on both sides, which is roughly consistent with the present-day topography of the Diable gorge. Given the blocky nature of the supply in

Figure 11. Initial glacial (squares) and present-day fluvial (circles) profiles for (a) Diable, (b) Etages, and (c) Gâ streams, and profile evolution predicted by the best fit transport-limited model ($m_s = n_s = 1$; K_s as indicated in the plots). Thick lines show profiles at 5 kyr intervals during the model run (dotted, 5 kyr; dashed-dotted, 10 kyr; dashed, 15 kyr; solid, 20 kyr).

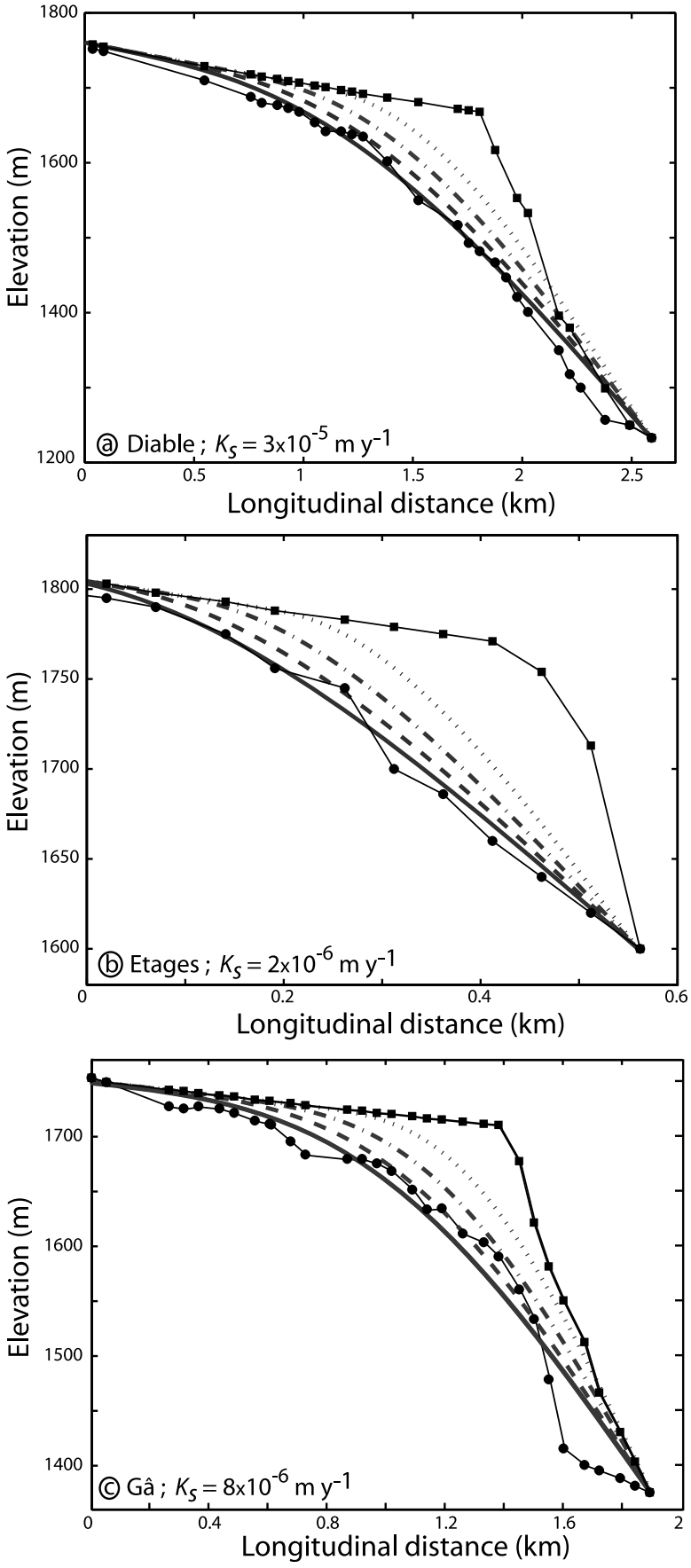
1800
1600
1400
1200
Elevation (m)
ⓐ Diable ; $K_S = 3x10^{-5}$ m y^{-1}
0
0.5
1
1.5
2
2.5
Longitudinal distance (km)
1800
1750
1700
1650
1600
Elevation (m)
ⓑ Etages ; $K_S = 2x10^{-6}$ m y^{-1}
0
0.2
0.4
0.6
Longitudinal distance (km)
1700
1600
1500
1400
Elevation (m)
© Gâ ; $K_S = 8x10^{-6}$ m y^{-1}
0
0.4
0.8
1.2
1.6
2
Longitudinal distance (km)

Figure 11

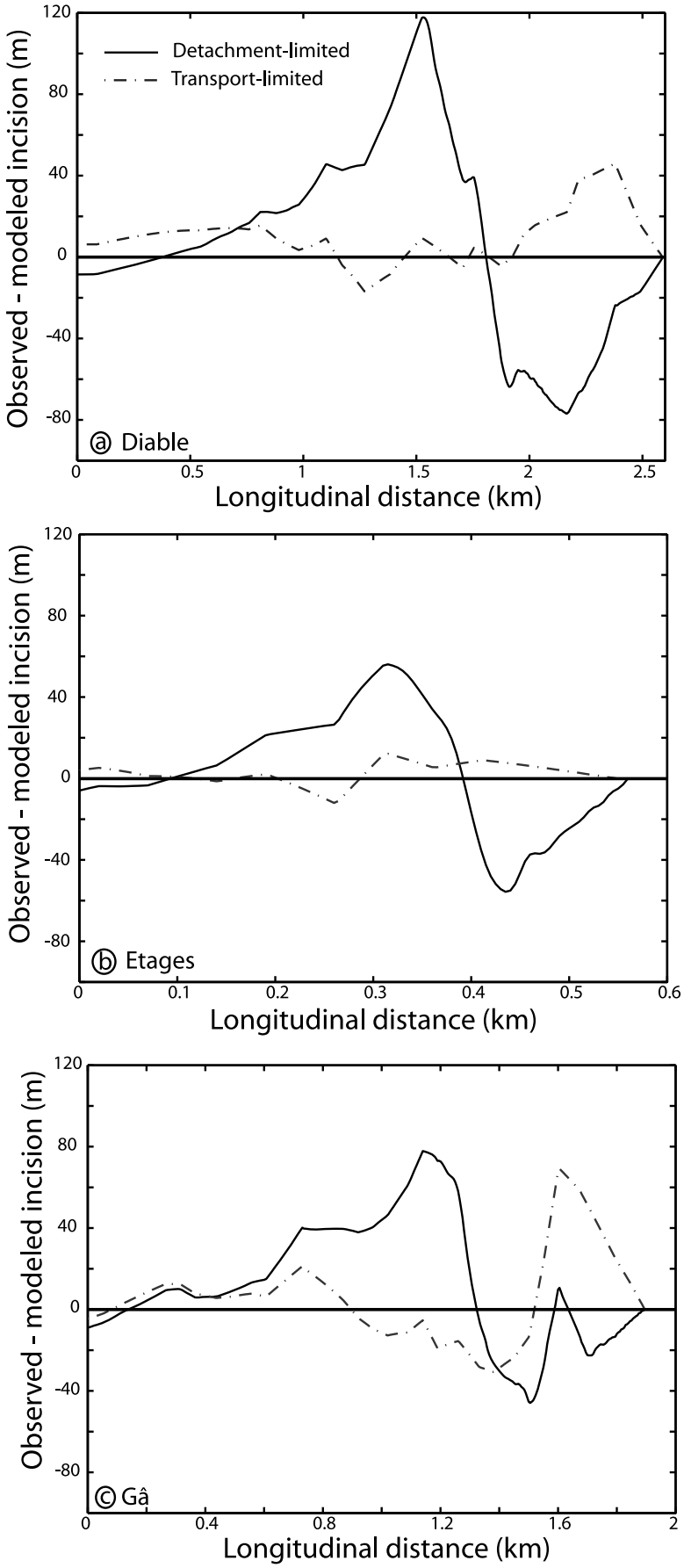
Detachment-limited
Transport-limited
Observed - modeled incision (m)
Longitudinal distance (km)
ⓐ Diable
ⓑ Etages
ⓒ Gâ
120
80
40
0
-40
-80
0
0.5
1
1.5
2
2.5
0.1
0.2
0.3
0.4
0.6
0.8
1.2
1.6

Figure 12

Table 1. Parameter Values for Diable Stream Using the Cover Model With and Without the Sediment Effect

Input Parameters	Diable River (Cover)	Diable River (Without Cover)
Dynamic cover effect, v	15	0
Static cover effect, ξ	0.4	0
Bank angle (°)	75	75
Manning coefficient	0.08	0.08
Bed load proportion (%)	50	/
Median grain size D_{50} (m)	0.5	0.5
Bed erosion factor K_{ref} (m^2 s kg^{-1})	1.6×10^{-11}	9.0×10^{-12}
Bed and wall critical shield stress	0.04	0.04
Wall erosion factor K_{bank} (m^2 s kg^{-1})	8.0×10^{-11}	5.0×10^{-12}
Sediment transport coefficient K_{sed} ($m^{5/2}$ s^2 $kg^{-3/2}$)	1.4×10^{-7}	/
Sediment supply rate coefficient Q_{wall} (mm yr^{-1})	9	/
Mean runoff, r (m y^{-1})	1	1
Discharge variability parameter, k[a]	1	1

[a]See *Lague et al.* [2005] and particularly equation (3) for details.

the gorge, we suppose that 50% of the volume of lateral sediment supply consists of bed load material. Assuming that 90% of the volume contributes to bed load would require gorge sidewall and hillslope erosion Q_{wall} of only 5 mm yr^{-1}.

[41] Preliminary simulations in which the lateral supply of sediment was spatially homogeneous led to unrealistic sedimentation (>30 m of sediment) upstream of the knickpoint. This led us to introduce Q_{wall} (see equation (A6)) to dynamically couple gorge incision and lateral sediment supply by gorge sidewall erosion. In this way, sediment supply increases in time, and varies spatially. We note that the resulting present-day pattern of sediment supply is in accord with the present-day pattern of in-channel deposits, which are more frequent in the gorge reach compared to the upstream reach of the stream. A difference arises at the lower reaches near the outlet where some of the rockfalls directly enter the trunk stream. This may explain the slight overprediction of mean sediment thickness (~5 m) in this location compared to the present-day configuration. As for the transport-limited model, this might also be due to the model not taking interactions with the trunk stream into account.

[42] The final part of the calibration requires finding the correct values for K_{ref}, K_{bank}, ξ, and v. The ratio of K_{ref} and K_{bank} strongly controls the predicted channel width, as well as the propagation rate of the knickpoint. Here ξ and v will mostly control how incision is attenuated downstream of the knickpoint. By trial and error, we find an optimal configuration (Figure 13b) leading to a low misfit between observed and predicted present-day stream profiles (RMS ~ 14.8 m) comparable to what we obtain with the transport-limited model. We note that final predicted widths and slopes are also realistic and range from a very steep (0.25–0.35 m m^{-1}) and narrow (around 10 m wide) channel in the gorge to a wider (15–20 m) channel with gentle slopes (0–0.01 m m^{-1}) upstream and downstream. This result requires both static and dynamic cover effects ($\xi = 0.4$, $v = 15$) to operate. The static cover effect is always more pronounced than the dynamic cover effect, representing in average 75% of bedrock incision inhibition at 2 kyr and up to 100% at the end of the simulation. A relatively strong to almost complete inhibition of incision by sediment transport downstream of the knickpoint is necessary to obtain satisfactory results, especially during the early stages of evolution. How exactly this inhibition operates is not clear. *Lague* [2010] shows that the variability of discharge and sediment supply significantly affects the long-term cover effect. The parameters related to this effect (variability of discharge, nonlinearity of the sediment supply law, see equation (A5)) are not well constrained for the type of small Alpine gorge we are studying. Also, the assumption of a single representative grain size may not well average the dynamics of an extremely skewed distribution of grain sizes. Hence we cannot rule out that the necessity to impose a relatively strong dynamic cover effect arises from incorrect parameterization of the sediment supply, transport and static cover effect.

[43] Despite the uncertainties on the nature of the inhibiting effect of sediment in the gorge, our numerical simulations support the notion that sediments play an important role in gorge deepening. The predicted profile evolution through time shows that gorges exhibit behavior that is close to that predicted by transport-limited models (Figure 13b) and that sediment flux from sidewalls has a major influence on fluvial incision dynamics [*Crosby et al.*, 2007; *Gasparini et al.*, 2007]. There are, however, two notable differences in the evolution of the transport-limited model and the cover model in terms of knickpoint propagation and present-day erosion rates. The cover model predicts the migration of a well defined knickpoint (Figure 13b) delimiting an upstream zone with no erosion, while the transport-limited model shows widespread erosion typical of diffusion behavior even at early stages, without a clearly defined knickpoint. We note that the transport-limited model does not predict the propagation of knickpoints, whereas these are observed in the upper reaches of the gorge. Another difference is that in the present-day configuration, incision is close to zero in the cover model (because of significant inhibition by sediment), while it is still ongoing in the transport limited model. In the cover model for instance, the first km of the gorge reaches a constant bedrock profile within 2–3 kyr, after which incision is inhibited by the sediment supply derived from upstream (Figure 13b). This difference in timing may have important implications for gorge evolution and sediment delivery to the trunk stream, and may

Figure 12. Difference between observed and modeled incision as a function of longitudinal distance for the transport- (dashed line) and detachment-limited (continuous line) models for (a) Diable, (b) Etages, and (c) Gâ streams.

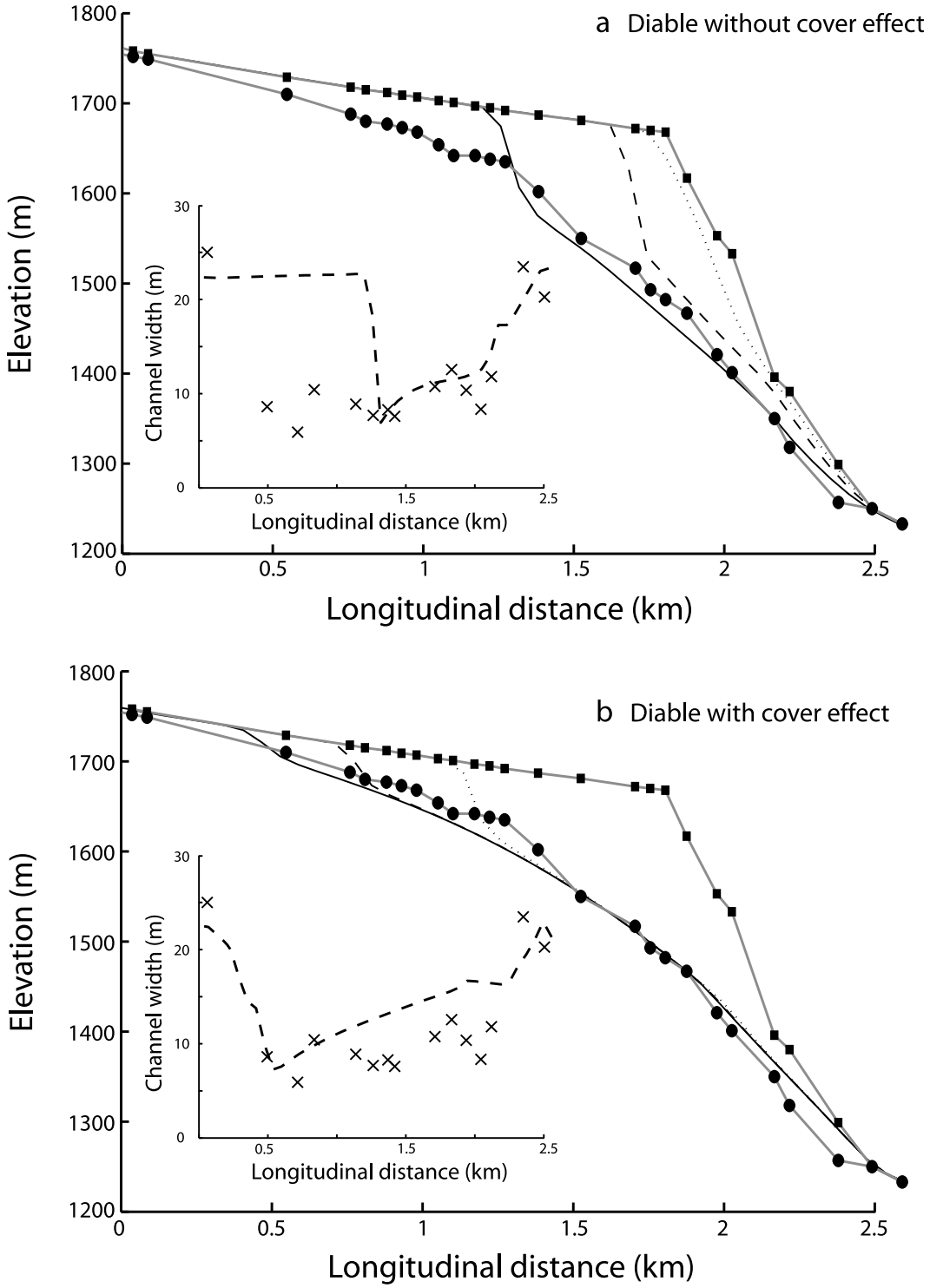

Figure 13. Initial glacial (squares) and present-day fluvial (circles) profiles for the Diable stream and predicted profile evolution for the cover model (a) without and (b) with the sediment cover effect. Lines show profiles at different times during the model run (dotted, 5 kyr; dashed, 10 kyr; solid, 20 kyr). Insets show predicted (dashed line) and observed (crosses) channel widths for present-day configuration.

help in differentiating which of the cover or transport-limited model governs postglacial gorge incision.

6. Discussion

[44] Our combined field, morphometric and numerical modeling approach provides insights into the fluvial evolution of bedrock gorges incising glacial hanging valleys. Based on field evidence, we show that these gorges mainly evolve by knickpoint diffusion through fluvial processes, starting from an abrupt glacial knickpoint. We quantified the glacial imprint on hanging valleys by studying the dependence of glacial hang heights on the ratio between tributary and trunk stream drainage area (Figure 5). This observation is consistent with the hypothesis that in glacial landscapes, hanging valleys mark the relative erosion capacities of the trunk and tributary glaciers [*MacGregor et al.*, 2000; *Amundson and Iverson*, 2006; *Anderson et al.*, 2006].

[45] Present-day gorge profiles were used to quantify fluvial incision processes. Field measurements highlight that gorge deepening is associated with channel narrowing and steep slopes (Figure 7). This observation suggests that high fluvial incision rates are accommodated by variations in both local gradients and channel geometry, especially channel width [*Turowski et al.*, 2006; *Wobus et al.*, 2006b; *Whittaker et al.*, 2007; *Snyder and Kammer*, 2008]. Mean gorge gradients (Figure 6) may reflect the incision and sediment transport capacity of tributary streams [*Wobus et al.*, 2006a] although inherited glacial controls on gorge gradients could not be excluded; subglacial controls have probably provided "initial" gorge gradients that further evolved through fluvial processes. By comparing glacial and present-day gorge profiles, we have made a first-order estimate of the maximum fluvial incision of these gorges (Figure 4). We have focused on knickpoint form and quantified the amount of knickpoint retreat for all gorges. Our results show that this retreat is correlated with the tributary drainage area (Figure 8), consistent with previous studies on knickpoint dynamics [*Bishop et al.*, 2005; *Crosby and Whipple*, 2006]. However, in contrast to *Crosby and Whipple* [2006], we have no indication that a threshold drainage area plays a role in maintaining knickpoint position, and in contrast to *Bishop et al.* [2005], who argued that this dependence implies detachment-limited incision, our modeling results indicate this not to be the case here.

[46] Our results show that knickpoint evolution takes place through "replacement-like" dynamics in which knickpoints evolve through horizontal retreat and vertical downwearing. *Gardner* [1983] suggests that this kind of evolution operates in a homogeneous substrate of intermediate resistance, where shear stress at the streambed is only slightly larger than the critical shear stress required for incision. In our case, lithologies vary from sedimentary cover rocks (marls and limestones) to crystalline bedrock (granites, gneisses and amphibolites). Morphometric results suggest that rates of gorge evolution may vary with lithology, although fluvial incision takes place by the same process of knickpoint replacement independent of lithology. The most striking lithological controls are observed for mean gorge gradients and knickpoint retreat rates. Bedrock gorges incising the more easily erodible sedimentary rocks are characterized by lower mean gradients and higher knickpoint retreat rates than gorges occurring in basement lithologies (Figures 6 and 8). A simple explanation could be that lower slopes correspond to a higher rate of overall gorge downwearing in the sedimentary rocks.

[47] Resolving the timing of onset of gorge incision has important implications for landscape evolution in response to glacial/interglacial conditions [*Korup and Schlunegger*, 2007]. Morphological evidence suggests that fluvial abrasion is one of the main processes operating in present-day gorge incision. This abrasion could potentially take place in either fluvial or subglacial conditions during glacial episodes. Moreover, field observations of inner gorges in the Swiss Alps revealed some evidence for periodic sediment infill during glacial stages [*Korup and Schlunegger*, 2007], supporting an older origin of bedrock gorges. On the contrary, *Valla et al.* [2009] recently reported cosmogenic data supporting Holocene postglacial incision of bedrock gorges; however this study focuses on a single bedrock gorge (the Diable) and others should be investigated to produce more data and better understand the postglacial evolution of these transient features.

[48] Assuming a coeval postglacial initiation of the gorges (i.e., younger than 20 kyr), estimated long-term incision rates from our morphometric results range between a minimum of 0.5 mm yr^{-1} and a maximum of 15 mm yr^{-1}. Such rates are high for fluvial processes in this lithological (sedimentary and crystalline rocks) and tectonic (the European Alps) setting. However, incision rates up to cm yr^{-1} have been inferred for transient fluvial reaches [*Whipple et al.*, 2000b] and have been reported for postglacial incision in the Western Alps from cosmogenic dating of fluvial terraces [*Brocard et al.*, 2003] and bedrock gorge sidewalls [*Valla et al.*, 2009]. Assuming a postglacial onset, temporally averaged knickpoint retreat rates lie between 2 and 200 mm yr^{-1} depending on drainage area; in agreement with values proposed in other fluvial settings [*Hayakawa and Matsukura*, 2003; *Bishop et al.*, 2005; *Lamb et al.*, 2007]. These studies and our results suggest that high fluvial incision rates can be encountered in disequilibrium contexts such as induced by glacial/interglacial climate oscillations.

[49] Numerical modeling has provided insights into the processes driving gorge deepening. We have shown that detachment-limited models, which consider incision rates to be limited by the incision capacity of the stream only, are not able to predict the observed gorge evolution. In contrast, transport-limited models, which consider that incision rates are limited by the capacity of the stream to carry sediments, predict the patterns of gorge deepening well, with relatively small misfits between modeled and observed profiles. Even though transport-limited models do not appear to be consistent with the relatively "resistant" lithologies and persistent knickpoints at time scales of 10^4 years [e.g., *Bishop and Goldrick*, 2000; *Bishop et al.*, 2005], the long-term behavior of bedrock gorges requires (close to) transport-limited conditions. A similar conclusion was reached by *Loget et al.* [2006] for knickpoints on much larger catchments. An alternative explanation for convex stream profiles associated with knickpoints was provided by *Haviv et al.* [2006], who suggest that they result from amplified erosion due to flow acceleration above waterfalls [*Berlin and Anderson*, 2009].

Although such a mechanism could explain the early evolution of the gorges we studied, when the glacial knickpoint is expressed as a free-falling waterfall (Figures 2a and 2b), most present-day gorges are not associated with waterfalls and drawdown of the knickpoint lip through this mechanism thus appears minimal or present only at a local step-pool scale.

[50] Detachment-limited models do not satisfactorily predict gorge evolution as their simple formulation does not take into account the evolution of channel geometry or sediment supply and transport. This supports the notion that even if present-day gorge incision appears to take place under detachment-limited conditions, the long-term dynamics differ and suggest high oscillations in sediment supply and thus sediment cover effect during gorge deepening [*Lague*, 2010]. Long-term gorge evolution thus depends on hillslope processes such as rockfalls, which can explain the diffusive component of knickpoint evolution and the presence of meter-scale blocks within the gorges. Moreover, debris flow incision may have occurred during gorge deepening, especially shortly after glacier retreat when sediment supply could have been important; morphological evidence does not suggest such processes for the recent gorge evolution, however.

[51] Transport-limited models do include potential sediment controls on bedrock incision; however the interaction between sediment transport and bedrock incision is included in a relatively simplistic manner. The use of more elaborate models thus appears required to fully explore the dynamics of stream incision. Such models should include a stochastic representation of stream discharges [*Tucker*, 2004; *Lague et al.*, 2005] as well as a full description of channel geometry [*Turowski et al.*, 2006; *Wobus et al.*, 2006b], and have to take into account the role of sediments in both limiting or increasing bedrock incision [*Sklar and Dietrich*, 2004, 2006; *Turowski et al.*, 2007]. However, the use of such models presupposes that all climatic, tectonic and hydraulic parameters controlling channel geometry and evolution can be estimated, which is clearly not the case in most situations.

[52] We have used the cover model to explore fluvial incision dynamics in more detail; this has highlighted the important role of an incision threshold, dynamic width adjustment and lateral sediment flux into the gorge. Slope failure events on the gorge sidewalls are required to provide relatively large amounts of sediment (up to 5–10 mm yr^{-1}) to the gorge stream. Meter-scale blocks are observed in the gorges (Figure 2d), suggesting that mass wasting mechanisms are active along gorge sidewalls and contribute significantly to lateral sediment supply into the river. Consequently, bedrock is partially protected from stream incision, reducing gorge deepening rates in a manner analogous to larger-scale examples described by *Korup et al.* [2006] and *Ouimet et al.* [2007]. Moreover, the hanging valleys we studied have small sizes (maximum drainage area of 40 km^2) and field evidence suggests that many large blocks have long residence times, as they are fluvially sculpted and differ from more recently produced and angular blocks. We thus suggest that present-day gorge incision mainly occurs during floods in spring (due to snowmelt) or summer (storms) that are capable of carrying and eroding such large blocks, thus leading to bedrock erosion. Similar to the dynamics exhibited in the modeling of *Lague* [2010], these frequent fluctuations of sediment supply and discharge entrain the system alternatively between detachment-limited behavior (when sediment deposits are negligible) and net deposition of sediment. At longer time scales, this propagates into a regime that can be close to a detachment-limited model if mean sediment supply is low or a transport-limited model if mean sediment supply is high [*Lague*, 2010].

[53] The ability of transport-limited and cover models to predict gorge evolution is also enhanced because they explicitly include spatial variations in channel geometry and its evolution through time [e.g., *Whittaker et al.*, 2007; *Snyder and Kammer*, 2008] (Figures 7 and 13) even though width evolution is empirically imposed from field measurements for the transport-limited models. The advantage of the cover model compared to transport-limited models is that it not only predicts vertical incision, but also potential width adjustments and sediment cover on the channel bed. Cover model simulations allow modeled and observed outcomes to be additionally tested using channel width and sediment thickness. They thereby allow further constraints on incision to be established.

7. Conclusions

[54] We conclude from our study that morphometric data combined with numerical fluvial incision models provides insights into gorge incision processes. Longitudinal profile reconstructions for both initial and present-day states allowed us to extract information on the formation of glacial hanging valleys and the incision of bedrock gorges. Our morphometric results support field evidence pointing to present-day fluvial incision of a formerly glaciated landscape. Field observations on active gorge channels suggest that fluvial abrasion is one of the main incision processes; however hillslope processes, in particular rockfalls from gorge sidewalls may provide substantial amounts of sediment to the gorge. Other processes such as subglacial abrasion, debris flows or incision during large floods cannot be excluded by our field observations. Assuming a postglacial initiation of gorge incision, we infer incision and knickpoint retreat rates that are not unrealistic compared to literature data. However, we cannot exclude an older origin of bedrock gorges in the light of morphological evidence and morphometric results.

[55] Numerical results clearly indicate that the long-term evolution of bedrock gorges cannot be caused by detachment-limited mechanisms alone. Numerical predictions suggest an important role for sediment supply and transport, but also for evolving channel geometry during gorge incision. We conclude from our numerical modeling that gorge incision can be modeled either by a simple transport-limited model, or by a complex model involving channel width evolution, discharge variability, strong inhibition by sediment transport and deposition downstream and tight coupling between gorge incision and sediment production from sidewall gorges and/or hillslopes. These results suggest that more detailed treatment of both channel geometry and sediment–bedrock interaction is required to capture the kinematics of gorge deepening. However, this requires detailed knowledge of past and present-day dynamics that is generally difficult to constrain. Our numerical results provide some insights into gorge incision process; however they do not clearly constrain the potential mechanisms acting in gorge incision and in bedrock

incision inhibition by sediment transport. We thus conclude that morphometric data and/or numerical modeling have to be used with caution to quantify erosion rates and landscape evolution; they must be combined with detailed field observations and absolute dating to capture the dynamics and timing of erosion processes and landscape evolution.

Appendix A: Description of the Cover Model

[56] The exact nature of the so-called cover effect and the adequate way to model it is still debated (see *Lague* [2010] for a review). Two types of modeling approach have been proposed: one in which the cover effect is expressed as a function of the ratio between the flux of bed load sediment Q_s and the bed load transport capacity Q_{eq} [*Beaumont et al.*, 1992; *Tucker and Slingerland*, 1994; *Sklar and Dietrich*, 2004; *Gasparini et al.*, 2007; *Turowski et al.*, 2007; *Chatanantavet and Parker*, 2008], and one in which the cover effect is expressed as a function of the mean thickness of sediment deposited on the bed [*Howard*, 1998; *Hancock and Anderson*, 2002; *Lague*, 2010]. It is not clear at present if these formulations represent different physical mechanisms of inhibition, and how they factor in elements of the complexity of the coupling between sediment transport, deposition and hydraulics (via roughness modifications). The effect of immobile alluvial deposits (called a static cover effect) on the bed has been demonstrated experimentally [*Sklar and Dietrich*, 2001; *Johnson and Whipple*, 2007], and is expected to translate into a dependence of the cover effect on the mean thickness of immobile sediment deposited on the bed [*Howard*, 1998; *Hancock and Anderson*, 2002; *Lague*, 2010]. The formulation of the cover effect using Q_s/Q_{eq} inherently fails to take into account any previous history of sediment stored on the bed [*Goode and Burbank*, 2009; *Lague*, 2010] and cannot be used at daily to yearly time scales alone. It can emerge as a long-term cover effect law when discharge and sediment supply stochasticity are factored in [*Lague*, 2010]; but it has also been advocated to model a so-called dynamic cover effect [*Turowski et al.*, 2007], in which mobile patches of sediment and increased near-bed sediment concentration reduces the bedrock surface exposed to incision at the time scales of single floods. This effect could be superimposed on the effect of immobile bed patches due to the presence of bed forms or different grain sizes.

[57] The cover model divides the stream channel into series of trapezoidal cross sections of fixed bank angle θ, linked together as in the work of *Stark* [2006]. In contrast to *Stark* [2006], we do not account for meandering effects as they are negligible in the study area. The model is driven by daily runoff events picked randomly from a probability distribution [*Lague et al.*, 2005] mimicking natural river flow variability at a daily time scale. In each section, daily discharge is equal to drainage area times daily runoff. As we do not have hydrological data for these gorges, we used mean runoff and variability typical of mountain environments (mean runoff $r = 1$ m yr^{-1}, discharge variability parameter $k = 1$) [*Lague et al.*, 2005]. For a given discharge and at each section, water depth is calculated using a Manning friction law, and corresponding mean bed and bank shear stresses (τ_{bed} and τ_{bank}, respectively) are computed using an experimentally derived law [*Knight et al.*, 1984; *Flintham and Carling*, 1988]. Corresponding mean bed incision and mean bank incision are computed using a simple shear stress incision law [e.g., *Howard and Kerby*, 1983; *Lavé and Avouac*, 2001]:

$$\dot{E} = K_x(\tau_x - \tau_{cx}), \text{ if } \tau_x > \tau_{cx}, \text{else } \dot{E}_x = 0. \quad \text{(A1)}$$

In equation (A1) the subscript x refers to bed or bank, and τ_{cx} corresponds to a critical shear stress (that we assume equal to the critical shear stress for incipient motion, see discussion by *Lague* [2010]). On the bed, K_{bed} in equation (A1) can be decreased by a static and/or a dynamic cover effect. According to the formulations used by *Lague* [2010], the resulting expression for K_{bed} is

$$K_{bed} = K_{ref} \exp\left(-\upsilon \frac{Q_s}{Q_{eq}}\right) \exp\left(-\frac{h_s}{\xi D_{50}}\right), \quad \text{(A2)}$$

where K_{ref} is a constant, v is a dynamic cover factor, h_s is the mean sediment thickness on the bed, D_{50} is the median grain diameter (estimated from field evidence), and ξ is a static cover factor. Given the very complex bed morphology of the gorges and the lack of a physical basis to set realistic values, we left ξ and v as free parameters in our simulations. Note that the exact expression for static and dynamic cover effects in equation (A2) does not change the overall dynamics of the model [see also *Lague* 2010]; although it would change the value of parameters inferred from modeling results (K_{ref} for instance). Using linearly decreasing laws [e.g., *Sklar and Dietrich*, 2004] would predict a similar channel evolution.

[58] The numerical model explicitly tracks the volume of sediment $Vol(x)$ deposited between two sections using the following equation:

$$\frac{dVol(x)}{dt} = Q_s(x - dx, t) + \beta q_{lat}(x, t)dx - Q_s(x, t), \quad \text{(A3)}$$

where t is time, β is the bed load fraction of the sediment supply, $q_{lat}(x,t)$ is the lateral supply of sediment per unit length of channel between x and $x - dx$ [see *Lague* 2010, Figure 2], dx is the distance between sections and $Q_s(x,t)$ is the total volumetric bed load flux at a distance x (x positive in the downstream direction). The volume of sediment stored is translated into a mean sediment thickness h_s assuming a packing density of 0.7. In equation (A3), $Q_s(x,t)$ can be limited by the transport capacity $Q_{eq}(x)$ of the section, estimated using a typical bed load sediment transport capacity law:

$$Q_{eq} = WK_{sed}(\tau_{bed} - \tau_{cbed})^{1.5}, \text{if } \tau_{bed} > \tau_{cbed}, \text{else } Q_{eq} = 0, \quad \text{(A4)}$$

where W is the flow width and K_{sed} is a transport efficiency coefficient. In equation (A4) the asymptotic scaling of transport capacity with shear stress is robust, and is predicted theoretically [e.g., *Bagnold*, 1977] and experimentally [e.g., *Meyer-Peter and Müller*, 1948; *Fernandez-Luque and van Beek*, 1976] in plane bed conditions (although a slightly higher exponent of 1.6 has been obtained by *Wong and Parker* [2006]). On the contrary, the value of K_{sed} and τ_{cbed} (or more commonly the critical shield stress τ_{cbed}*) is not universal. In steep gorges with significant protruding blocks and bed form roughness, the prediction of K_{sed} and τ_{cbed}* is challenging and does not yield universal parameters [*Yager et al.*, 2007; *Lamb et al.*, 2008b]. Hence we allow K_{sed} to be significantly smaller than the typical value predicted by the *Wong and Parker* [2006] law ($K_{sed} \sim 5.10^{-6}$ m$^{5/2}$ s^2 kg$^{-3/2}$ in that

case) while we arbitrarily fix $\tau_{cbed}^* = 0.04$. The median grain size D_{50} is set to 50 cm, which is close to the median size of sediments found in the gorges (including meter-scale blocks).

[59] In these simulations, sediment is supplied to the river at each cross section by lateral supply $q_{lat}(x)$ from gorge wall and hillslope erosion. As in the work of *Lague* [2010] this supply of sediment varies stochastically with the daily variation of runoff according to a one to one relationship:

$$q_{lat}(x,t) = k_{sup}(x,t)Q^*(t)^m, \quad \text{(A5)}$$

in which $k_{sup}(x)$ can vary longitudinally and $Q^*(t)$ is the normalized runoff (i.e., the daily runoff divided by mean annual runoff). We use $m = 2$, although we do not have any constraint on this parameter. As discussed in the text, it rapidly became clear that a realistic profile evolution required the supply of sediment to vary along the stream. We basically interpret this effect as wall collapse and erosion due to gorge incision. To factor in this effect, we couple lateral sediment supply to the total local incision since the beginning of the simulation:

$$k_{sup}(x,t) = 2(h(x,t) - h(x,0))Q_{wall}, \quad \text{(A6)}$$

Where $h(x,t)$ is the local bed elevation at time t and Q_{wall} is the mean sidewall erosion rate. Equation (A6) mimics parallel retreat of the two sidewalls of the gorge leading to higher sediment supply where the channel is incising most rapidly. Slope stability modeling [*Korup and Schlunegger*, 2007] supports this approach: the higher the gorge sidewalls, the less stable they are and the more sediment they produce. We acknowledge that equation (A6) is likely oversimplified and could be for instance more nonlinear, but it does dynamically couple gorge deepening and sidewall erosion with only one parameter.

[60] Finally, channel geometry is altered at daily time steps as a function of mean bed and bank incision, keeping the bank angle fixed. For instance, if $E_{bank} > E_{bed}\cos\theta$, the channel widens, whereas if $E_{bank} = E_{bed}\cos\theta$ the channel width is not modified. As demonstrated by *Stark* [2006], this simple model allows for a dynamic (and implicit) variation of channel width.

[61] **Acknowledgments.** This study represent P.V.'s MSc project at Université Joseph Fourier and forms part of two projects on Quaternary relief development and denudation rates in the Western Alps (P. van der Beek) and drainage network dynamics (D. Lague) funded by the INSU-CNRS Reliefs de la Terre program. We thank reviewers Simon Brocklehurst, Oliver Korup, Michael Lamb, an anonymous reviewer, and Associate Editor Brian MacArdell for thorough and constructive reviews that helped to significantly improve the manuscript.

References

Alley, R. B., D. E. Lawson, G. J. Larson, E. B. Evenson, and G. S. Baker (2003), Stabilizing feedbacks in glacier-bed erosion, *Nature*, *424*, 758–760, doi:10.1038/nature01839.

Amerson, B., D. R. Montgomery, and G. Meyer (2008), Relative size of glacial and fluvial valleys in central Idaho, *Geomorphology*, *93*, 537–547, doi:10.1016/j.geomorph.2007.04.001.

Amundson, J. M., and N. R. Iverson (2006), Testing a glacial erosion rule using hang heights of hanging valleys, Jasper National Park, Alberta, Canada, *J. Geophys. Res.*, *111*, F01020, doi:10.1029/2005JF000359.

Anderson, R. S. (1994), Evolution of the Santa Cruz Mountains, California, through tectonic growth and geomorphic decay, *J. Geophys. Res.*, *99*, 20,161–20,180, doi:10.1029/94JB00713.

Anderson, R. S., P. Molnar, and M. A. Kessler (2006), Features of glacial valley profiles simply explained, *J. Geophys. Res.*, *111*, F01004, doi:10.1029/2005JF000344.

Bagnold, R. A. (1977), Bed load transport by natural rivers, *Water Resour. Res.*, *13*, 303–312, doi:10.1029/WR013i002p00303.

Beaumont, C., P. Fullsack, and J. Hamilton (1992), Erosional control of active compressional orogens, in *Thrust Tectonics*, edited by K. R. McClay, pp. 1–18, Chapman and Hall, New York.

Berlin, M. M., and R. S. Anderson (2007), Modeling of knickpoint retreat on the Roan Plateau, western Colorado, *J. Geophys. Res.*, *112*, F03S06, doi:10.1029/2006JF000553.

Berlin, M. M., and R. S. Anderson (2009), Steepened channels upstream of knickpoints: Controls on relict landscape response, *J. Geophys. Res.*, *114*, F03018, doi:10.1029/2008JF001148.

Bishop, P., and G. Goldrick (2000), Geomorphological evolution of the East Australian continental margin, in *Geomorphology and Global Tectonics*, edited by M. A. Summerfield, pp. 225–254, John Wiley, New York.

Bishop, P., T. B. Hoey, J. D. Jansen, and I. L. Artza (2005), Knickpoint recession rate and catchment area: The case of uplifted rivers in eastern Scotland, *Earth Surf. Processes Landforms*, *30*(6), 767–778, doi:10.1002/esp.1191.

Brocard, G. Y., P. A. van der Beek, D. L. Bourles, L. L. Siame, and J. L. Mugnier (2003), Long-term fluvial incision rates and postglacial river relaxation time in the French Western Alps from ^{10}Be dating of alluvial terraces with assessment of inheritance, soil development and wind ablation effects, *Earth Planet. Sci. Lett.*, *209*, 197–214, doi:10.1016/S0012-821X(03)00031-1.

Brocklehurst, S. H., and K. X. Whipple (2002), Glacial erosion and relief production in the eastern Sierra Nevada, California, *Geomorphology*, *42*, 1–24, doi:10.1016/S0169-555X(01)00069-1.

Cederbom, C. E., H. D. Sinclair, F. Schlunegger, and M. K. Rahn (2004), Climate-induced rebound and exhumation of the European Alps, *Geology*, *32*, 709–712, doi:10.1130/G20491.1.

Champagnac, J. D., P. Molnar, R. S. Anderson, C. Sue, and B. Delacou (2007), Quaternary erosion-induced isostatic rebound in the Western Alps, *Geology*, *35*, 195–198, doi:10.1130/G23053A.1.

Chatanantavet, P., and G. Parker (2008), Experimental study of bedrock channel alluviation under varied sediment supply and hydraulic conditions, *Water Resour. Res.*, *44*, W12446, doi:10.1029/2007WR006581.

Crosby, B. T., and K. X. Whipple (2006), Knickpoint initiation and distribution within fluvial networks: 236 waterfalls in the Waipaoa River, North Island, New Zealand, *Geomorphology*, *82*, 16–38, doi:10.1016/j.geomorph.2005.08.023.

Crosby, B. T., K. X. Whipple, N. M. Gasparini, and C. W. Wobus (2007), Formation of fluvial hanging valleys: Theory and simulation, *J. Geophys. Res.*, *112*, F03S10, doi:10.1029/2006JF000566.

Dumont, T., J. D. Champagnac, C. Crouzet, and P. Rochat (2008), Multistage Alpine shortening in central Dauphiné (French Western Alps): Implications for pre-Alpine restoration, *Swiss J. Geosci.*, *101*, 89–110, doi:10.1007/s00015-008-1280-2.

Duvall, A., E. Kirby, and D. Burbank (2004), Tectonic and lithologic controls on bedrock channel profiles and processes in coastal California, *J. Geophys. Res.*, *109*, F03002, doi:10.1029/2003JF000086.

Fernandez-Luque, R., and R. van Beek (1976), Erosion and transport of bed-load sediment, *J. Hydraul. Res.*, *14*, 127–144.

Finnegan, N. J., G. Roe, D. R. Montgomery, and B. Hallet (2005), Controls on the channel width of rivers: Implications for modeling fluvial incision of bedrock, *Geology*, *33*, 229–232, doi:10.1130/G21171.1.

Flintham, T. P., and P. A. Carling (1988), The prediction of mean bed and wall boundary shear in uniform and compositely roughened channels, in *International Conference on River Regime*, edited by W. P. White, pp. 267–287, John Wiley, Chichester, U. K.

Ford, M. (1996), Kinematics and geometry of early Alpine, basement involved folds, SW Pelvoux Massif, SE France, *Eclogae Geol. Helv.*, *89*, 269–295.

Frankel, K. L., F. J. Pazzaglia, and J. D. Vaughn (2007), Knickpoint evolution in a vertically bedded substrate, upstream-dipping terraces, and Atlantic slope bedrock channels, *Geol. Soc. Am. Bull.*, *119*, 476–486, doi:10.1130/B25965.1.

Gardner, T. W. (1983), Experimental study of knickpoint and longitudinal profile evolution in cohesive, homogeneous material, *Geol. Soc. Am. Bull.*, *94*, 664–672, doi:10.1130/0016-7606(1983)94<664:ESOKAL>2.0.CO;2.

Gasparini, N. M., K. X. Whipple, and R. L. Bras (2007), Predictions of steady state and transient landscape morphology using sediment-flux-dependent river incision models, *J. Geophys. Res.*, *112*, F03S09, doi:10.1029/2006JF000567.

Goldrick, G., and P. Bishop (2007), Regional analysis of bedrock stream long profiles: Evaluation of Hack's SL form, and formulation and assessment of an alternative (the DS form), *Earth Surf. Processes Landforms*, *32*(5), 649–671, doi:10.1002/esp.1413.

Goode, J. K., and D. W. Burbank (2009), Numerical study of degradation of fluvial hanging valleys due to climate change, *J. Geophys. Res.*, *114*, F01017, doi:10.1029/2007JF000965.

Gudmundsson, G. H. (1994), An order of magnitude estimate of the current uplift rates in Switzerland caused by the Würm alpine deglaciation, *Eclogae Geol. Helv.*, *87*, 545–557.

Hallet, B. (1996), Glacial quarrying: A simple theoretical model, *Ann. Glaciol.*, *22*, 1–8.

Hancock, G. S., and R. S. Anderson (2002), Numerical modeling of fluvial terrace formation in response to oscilating climate, *Geol. Soc. Am. Bull.*, *114*, 1131–1142.

Harbor, J. M. (1995), Development of glacial-valley cross sections under conditions of spatially variable resistance to erosion, *Geomorphology*, *14*, 99–107, doi:10.1016/0169-555X(95)00051-1.

Harkins, N., E. Kirby, A. Heimsath, R. Robinson, and U. Reiser (2007), Transient fluvial incision in the headwaters of the Yellow River, northeastern Tibet, China, *J. Geophys. Res.*, *112*, F03S04, doi:10.1029/2006JF000570.

Haviv, I., Y. Enzel, K. X. Whipple, E. Zilberman, J. Stone, A. Matmon, and L. K. Fifield (2006), Amplified erosion above waterfalls and oversteepened bedrock reaches, *J. Geophys. Res.*, *111*, F04004, doi:10.1029/2006JF000461.

Hayakawa, Y., and Y. Matsukura (2003), Recession rates of waterfalls in Boso Peninsula, Japan, and a predictive equation, *Earth Surf. Processes Landforms*, *28*(6), 675–684, doi:10.1002/esp.519.

Hinderer, M. (2001), Late Quaternary denudation of the Alps, valley and lake fillings and modern river loads, *Geodin. Acta*, *14*(4), 231–263, doi:10.1016/S0985-3111(01)01070-1.

Howard, A. D. (1998), Long profile developpement of bedrock channels: Interaction of weathering, mass wasting, bed erosion, and sediment transport, in *Rivers Over Rock: Fluvial Processes in Bedrock Channels*, *Geophys. Monogr. Ser.*, vol. 107, edited by K. J. Tinkler and E. E. Wohl, pp. 297–319, AGU, Washington, D. C.

Howard, A. D., and G. Kerby (1983), Channel changes in badlands, *Geol. Soc. Am. Bull.*, *94*, 739–752, doi:10.1130/0016-7606(1983)94<739:CCIB>2.0.CO;2.

Howard, A. D., W. E. Dietrich, and M. A. Seidl (1994), Modeling fluvial erosion on regional to continental scales, *J. Geophys. Res.*, *99*, 13,971–13,986, doi:10.1029/94JB00744.

Ivy-Ochs, S., J. Schäfer, P. W. Kubik, H. A. Synal, and C. Schlüchter (2004), Timing of deglaciation on the northern Alpine foreland (Switzerland), *Eclogae Geol. Helv.*, *97*, 47–55, doi:10.1007/s00015-004-1110-0.

Johnson, J. P., and K. X. Whipple (2007), Feedbacks between erosion and sediment transport in experimental bedrock channels, *Earth Surf. Processes Landforms*, *32*(7), 1048–1062, doi:10.1002/esp.1471.

Johnson, J. P. L., K. X. Whipple, L. S. Sklar, and T. C. Hanks (2009), Transport slopes, sediment cover, and bedrock channel incision in the Henry Mountains, Utah, *J. Geophys. Res.*, *114*, F02014, doi:10.1029/2007JF000862.

Jouanne, F., G. Ménard, and X. Darmendrail (1995), Present-day vertical displacements in the north-Western Alps and southern Jura Mountains: Data from levelling comparisons, *Tectonics*, *14*, 606–616, doi:10.1029/94TC03336.

Kahle, H. G., et al. (1997). Recent crustal movements, geoid and density distribution: Contribution from integrated satellite and terrestrial measurements, in *Results of the National Research Program*, vol. 20, O. A. Pfiffner et al., pp. 251–259, Birkhäuser, Basel, Switzerland.

Kirby, E., and K. Whipple (2001), Quantifying differential rock-uplift rates via stream profile analysis, *Geology*, *29*, 415–418, doi:10.1130/0091-7613(2001)029<0415:QDRURV>2.0.CO;2.

Knight, D. W., J. D. Demetrious, and M. E. Hamed (1984), Boundary shear in smooth rectangular channels, *J. Hydraul. Div. Am. Soc. Civ. Eng.*, *110*(4), 405–422, doi:10.1061/(ASCE)0733-9429(1984)110:4(405).

Kooi, H., and C. Beaumont (1996), Large-scale geomorphology: Classical concepts reconciled and integrated with contemporary ideas via a surface processes model, *J. Geophys. Res.*, *101*, 3361–3386, doi:10.1029/95JB01861.

Koppes, M. N., and D. R. Montgomery (2009), The relative efficacy of fluvial and glacial erosion over modern to orogenic timescales, *Nat. Geosci.*, *2*, 644–647, doi:10.1038/ngeo616.

Korup, O., and F. Schlunegger (2007), Bedrock landsliding, river incision, and transience of geomorphic hillslope-channel coupling: Evidence from inner gorges in the Swiss Alps, *J. Geophys. Res.*, *112*, F03027, doi:10.1029/2006JF000710.

Korup, O., A. L. Strom, and J. T. Weidinger (2006), Fluvial response to large rock-slope failures: Examples from the Himalayas, the Tien Shan, and the Southern Alps in New Zealand, *Geomorphology*, *78*, 3–21.

Lague, D. (2010), Reduction of long-term bedrock incision efficiency by short-term alluvial cover intermittency, *J. Geophys. Res.*, *115*, F02011, doi:10.1029/2008JF001210.

Lague, D., N. Hovius, and P. Davy (2005), Discharge, discharge variability, and the bedrock channel profile, *J. Geophys. Res.*, *110*, F04006, doi:10.1029/2004JF000259.

Lamb, M. P., A. D. Howard, W. E. Dietrich, and J. T. Perron (2007), Formation of amphitheater-headed valleys by waterfall erosion after large-scale slumping on Hawai'i, *Geol. Soc. Am. Bull.*, *119*, 805–822, doi:10.1130/B25986.1.

Lamb, M. P., W. E. Dietrich, and L. S. Sklar (2008a), A model for fluvial bedrock incision by impacting suspended and bedload sediment, *J. Geophys. Res.*, *113*, F03025, doi:10.1029/2007JF000915.

Lamb, M. P., W. E. Dietrich, and J. G. Venditti (2008b), Is the critical Shields stress for incipient sediment motion dependent on channel-bed slope?, *J. Geophys. Res.*, *113*, F02008, doi:10.1029/2007JF000831.

Lavé, J., and J. P. Avouac (2001), Fluvial incision and tectonic uplift across the Himalayas of central Nepal, *J. Geophys. Res.*, *106*, 26,561–26,591, doi:10.1029/2001JB000359.

Leloup, P. H., N. Arnaud, E. R. Sobel and R. Lacassin (2005), Alpine thermal and structural evolution of the highest external crystalline massif: The Mont Blanc, *Tectonics*, *24*, TC4002, doi:10.1029/2004TC001676.

Lindsay, J. B. (2005), The terrain analysis system: A tool for hydro-geomorphic applications, *Hydrol. Processes*, *19*, 1123–1130, doi:10.1002/hyp.5818.

Loget, N., P. Davy, and J. Van Den Driessche (2006), Mesoscale fluvial erosion parameters deduced from modeling the Mediterranean sea level drop during the Messinian (late Miocene), *J. Geophys. Res.*, *111*, F03005, doi:10.1029/2005JF000387.

MacGregor, K. R., R. S. Anderson, S. P. Anderson, and E. D. Waddington (2000), Numerical simulations of glacial-valley longitudinal profile evolution, *Geology*, *28*, 1031–1034, doi:10.1130/0091-7613(2000)28<1031:NSOGLP>2.0.CO;2.

Meyer-Peter, E., and R. Müller (1948), Formulas for bed-load transport, paper presented at 2nd Congress of IAHR, Stockholm, Sweden.

Montgomery, D. R. (2002), Valley formation by fluvial and glacial erosion, *Geology*, *30*, 1047–1050, doi:10.1130/0091-7613(2002)030<1047:VFBFAG>2.0.CO;2.

Montgomery, D. R., and J. M. Buffington (1997), Channel-reach morphology in mountain drainage basins, *Geol. Soc. Am. Bull.*, *109*, 596–611, doi:10.1130/0016-7606(1997)109<0596:CRMIMD>2.3.CO;2.

Montjuvent, G. (1978), *Le Drac. Morphologie, stratigraphie et chronologie quaternaires d'un bassin alpin. Editions du CNRS*, 433 pp., Cent. Natl. de la Rech. Sci., Paris.

Naylor, S., and E. J. Gabet (2007), Valley asymmetry and glacial versus nonglacial erosion in the Bitterroot Range, Montana, USA, *Geology*, *35*, 375–378, doi:10.1130/G23283A.1.

Nicoud, G., G. Royer, J.-C. Corbin, F. Lemeille, and A. Paillet (2002), Glacial erosion and infilling of the Isère valley during the recent Quaternary: New results from borehole GMB1 in the Grenoble area (France), *Geol. Fr.*, *4*, 39–50.

Niemann, J. D., N. M. Gasparini, G. E. Tucker, and R. L. Bras (2001), A quantitative evaluation of Playfair's law and its use in testing long-term stream erosion models, *Earth Surf. Processes Landforms*, *26*, 1317–1332, doi:10.1002/esp.272.

Ouimet, W. B., K. X. Whipple, L. H. Royden, Z. Sun, and Z. Chen (2007), The influence of large landslides on river incision in a transient landscape: Eastern margin of the Tibetan Plateau (Sichuan, China), *Geol. Soc. Am. Bull.*, *119*, 1462–1476, doi:10.1130/B26136.1.

Press, W. H., S. A. Teukolsky, W. T. Vetterling, and B. P. Flannery (1992), *Numerical Recipes in FORTRAN 77: The Art of Scientific Computing*, 921 pp., Cambridge Univ. Press, New York.

Schlunegger, F., and H. Schneider (2005), Relief-rejuvenation and topographic length scales in a fluvial drainage basin, Napf area, central Switzerland, *Geomorphology*, *69*, 102–117, doi:10.1016/j.geomorph.2004.12.008.

Sklar, L. S., and W. E. Dietrich (1998), River longitudinal profiles and bedrock incision models: Stream power and the influence of sediment supply, in *Rivers Over Rock: Fluvial Processes in Bedrock Channels*, *Geophys. Monogr. Ser.*, vol. 107, edited by K. J. Tinkler and E. E. Wohl, pp. 237–260, AGU, Washington, D. C.

Sklar, L. S., and W. E. Dietrich (2001), Sediment and rock strength controls on river incision into bedrock, *Geology*, *29*, 1087–1090, doi:10.1130/0091-7613(2001)029<1087:SARSCO>2.0.CO;2.

Sklar, L. S., and W. E. Dietrich (2004), A mechanistic model for river incision into bedrock by saltating bed load, *Water Resour. Res.*, *40*, W06301, doi:10.1029/2003WR002496.

Sklar, L., and W. E. Dietrich (2006), The role of sediment in controlling steady state bedrock channel slope: Implications of the saltation-abrasion

incision model, *Geomorphology*, *82*, 58–83, doi:10.1016/j.geomorph.2005.08.019.

Snyder, N. P., and L. L. Kammer (2008), Dynamic adjustments in channel width in response to a forced diversion: Gower Gulch, Death Valley National Park, *Calif. Geol.*, *36*(2), 187–190.

Stark, C. P. (2006), A self-regulating model of bedrock river channel geometry, *Geophys. Res. Lett.*, *33*, L04402, doi:10.1029/2005GL023193.

Stock, J. D., and W. E. Dietrich (2003), Valley incision by debris flows: Evidence of a topographic signature, *Water Resour. Res.*, *39*(4), 1089, doi:10.1029/2001WR001057.

Stock, J. D., and D. R. Montgomery (1999), Geologic constraints on bedrock river incision using the stream power law, *J. Geophys. Res.*, *104*(B3), 4983–4993, doi:10.1029/98JB02139.

Tomkin, J. H., M. T. Brandon, F. J. Pazzaglia, J. R. Barbour, and S. D. Willett (2003), Quantitative testing of bedrock incision models for the Clearwater River, NW Washington State, *J. Geophys. Res.*, *108*(B6), 2308, doi:10.1029/2001JB000862.

Tucker, G. E. (2004), Drainage basin sensitivity to tectonic and climatic forcing: Implications of a stochastic model for the role of entrainment and erosion thresholds, *Earth Surf. Processes Landforms*, *29*(2), 185–205, doi:10.1002/esp.1020.

Tucker, G. E., and R. L. Slingerland (1994), Erosional dynamics, flexural isostasy, and long-lived escarpments: A numerical modeling study, *J. Geophys. Res.*, *99*, 12,229–212,243.

Tucker, G. E., and K. X. Whipple (2002), Topographic outcomes predicted by stream erosion models: Sensitivity analysis and intermodel comparison, *J. Geophys. Res.*, *107*(B9), 2179, doi:10.1029/2001JB000162.

Turowski, J. M., D. Lague, A. Crave, and N. Hovius (2006), Experimental channel response to tectonic uplift, *J. Geophys. Res.*, *111*, F03008, doi:10.1029/2005JF000306.

Turowski, J. M., D. Lague, and N. Hovius (2007), Cover effect in bedrock abrasion: A new derivation and its implications for the modeling of bedrock channel morphology, *J. Geophys. Res.*, *112*, F04006, doi:10.1029/2006JF000697.

Valla, P. G., P. A. van der Beek, and J. Carcaillet (2009), Dating bedrock gorge incision in the French Western Alps, (Ecrins-Pelvoux massif) using cosmogenic ^{10}Be, *Terra Nova*, *22*, 18–25.

van der Beek, P., and P. Bishop (2003), Cenozoic river profile development in the Upper Lachlan catchment (SE Australia) as a test of quantitative fluvial incision models, *J. Geophys. Res.*, *108*(B6), 2309, doi:10.1029/2002JB002125.

Vernon, A. J., P. A. van der Beek, H. D. Sinclair, and M. K. Rahn (2008), Increase in late Neogene denudation of the European Alps confirmed by analysis of a fission track thermochronology database, *Earth Planet. Sci. Lett.*, *270*, 316–329, doi:10.1016/j.epsl.2008.03.053.

Weissel, J. K., and M. A. Seidl (1998), Inland propagation of erosional escarpments and river profile evolution across the southeast Australian passive continental margin, in *Rivers Over Rock: Fluvial Processes in Bedrock Channels, Geophys. Monogr. Ser.*, vol. 107, edited by K. J. Tinkler and E. E. Wohl, pp. 189–206, AGU, Washington, D. C.

Whipple, K. X., and G. E. Tucker (1999), Dynamics of the stream-power river incision model: Implications for height limits of mountain ranges, landscape response timescales, and research needs, *J. Geophys. Res.*, *104*, 17,661–17,674, doi:10.1029/1999JB900120.

Whipple, K. X., and G. E. Tucker (2002), Implications of sediment-flux-dependent river incision models for landscape evolution, *J. Geophys. Res.*, *107*(B2), 2039, doi:10.1029/2000JB000044.

Whipple, K. X., E. Kirby, and S. H. Brocklehurst (1999), Geomorphic limits to climate-induced increases in topographic relief, *Nature*, *401*, 39–43, doi:10.1038/43375.

Whipple, K. X., G. S. Hancock, and R. S. Anderson (2000a), River incision into bedrock: Mechanics and relative efficacy of plucking, abrasion, and cavitation, *Geol. Soc. Am. Bull.*, *112*, 490–503, doi:10.1130/0016-7606(2000)112<490:RIIBMA>2.0.CO;2.

Whipple, K. X., N. P. Snyder, and K. Dollenmayer (2000b), Rates and processes of bedrock incision by the Upper Ukak River since the 1912 Novarupta ash flow in the Valley of Ten Thousand Smokes, Alaska, *Geology*, *28*, 835–838, doi:10.1130/0091-7613(2000)28<835:RAPOBI>2.0.CO;2.

Whittaker, A. C., P. A. Cowie, M. Attal, G. E. Tucker, and G. P. Roberts (2007), Bedrock channel adjustment to tectonic forcing: Implications for predicting river incision rates, *Geology*, *35*, 103–106, doi:10.1130/G23106A.1.

Willett, S. D. (1999), Orogeny and orography: The effects of erosion on the structure of mountain belts, *J. Geophys. Res.*, *104*, 28,957–28,981, doi:10.1029/1999JB900248.

Willgoose, G. R., R. L. Bras, and I. Rodriguez-Iturbe (1991), A physically based coupled network growth and hillslope evolution model: 1. Theory, *Water Resour. Res.*, *27*, 1671–1684, doi:10.1029/91WR00935.

Wobus, C. W., B. T. Crosby, and K. X. Whipple (2006a), Hanging valleys in fluvial systems: Controls on occurrence and implications for landscape evolution, *J. Geophys. Res.*, *111*, F02017, doi:10.1029/2005JF000406.

Wobus, C. W., G. E. Tucker, and R. S. Anderson (2006b), Self-formed bedrock channels, *Geophys. Res. Lett.*, *33*, L18408, doi:10.1029/2006GL027182.

Wohl, E. E., and D. M. Merritt (2001), Bedrock channel morphology, *Geol. Soc. Am. Bull.*, *113* 1205–1212, doi:10.1130/0016-7606(2001)113<1205:BCM>2.0.CO;2.

Wong, M., and G. Parker (2006), Reanalysis and correction of bed-load relation of Meyer-Peter and Müller using their own database, *J. Hydraul. Eng.*, *132*(11), 1159–1168, doi:10.1061/(ASCE)0733-9429(2006)132:11(1159).

Yager, E. M., J. W. Kirchner, and W. E. Dietrich (2007), Calculating bed load transport in steep boulder bed channels, *Water Resour. Res.*, *43*, W07418, doi:10.1029/2006WR005432.

D. Lague, Géosciences Rennes, Université Rennes 1, CNRS, Campus de Beaulieu, F-35042 Rennes, France.

P. G. Valla and P. A. van der Beek, Laboratoire de Géodynamique des Chaînes Alpines, Université Joseph Fourier, BP 53, F-38041 Grenoble, France. (pierre.valla@e.ujf-grenoble.fr)